Earth-Science Reviews 237 (2023) 104328

Contents lists available at ScienceDirect

Earth-Science Reviews

journal homepage: www.elsevier.com/locate/earscirev

Cenozoic exhumation in the Mediterranean and the Middle East

Riccardo Lanari [a,b,*], Alex Boutoux [b], Claudio Faccenna [b,c], Frederic Herman [d], Sean D. Willett [e], Paolo Ballato [b]

[a] Department of Earth Sciences, University of Florence, Italy
[b] Department of Science, Roma Tre University, Roma, Italy
[c] GFZ, German Research Center for Geoscience, Germany
[d] Institute of Earth Surface Dynamics, University of Lausanne, Switzerland
[e] ETH Zurich, Department of Earth Sciences, Zurich, Switzerland

ARTICLE INFO

Keywords:
Thermochronometric data compilation
Inferred exhumation rates
Inversion method
Continental collision
Climate forcing

ABSTRACT

We investigate the processes driving spatial-temporal patterns of Cenozoic exhumation in the Mediterranean and the Middle East by compiling >7300 published low-temperature thermochronometric ages and converting them into exhumation rates through a formal inversion process based on thermal modeling and closure temperature kinetics. Exhumation rates are resolved using piecewise-continuous spatial variability and timesteps of five million years. The spatial variability of the inferred rates is constrained by a plate tectonic reconstruction based on the integration of available kinematic data. In this model we recognize different tectonic blocks with a relative homogenous tectono-sedimentary and tectono-magmatic history. The inverted erosion rates for each block are then compared with regional and local geodynamic rates, eustatic curves, and climatic forcing to decipher common patterns and possible teleconnections among different blocks. The results document asynchronous exhumation across different tectonic blocks indicating local (i.e., at the scale of a single orogen) rather than regional (i.e., at the scale of multiple orogens) control on erosion rates. The main processes driving exhumation include collisions of Arabia, Adria, and Iberia with Eurasia, and subduction and retreat of the various Neo-Tethys slabs and back-arc basins. Specifically, we recognize two tectonic domains: collisional deformation zones where exhumation is controlled by surface uplift and erosion, and back-arcs areas where exhumation is controlled by tectonic denudation. In both cases we observe an increase in mean rates and rate variance during tectonic activity, followed by a decrease in each metric as tectonic activity wanes. Finally, we note (with a few exceptions) an overall increase in exhumation rates over most of the Mediterranean and Middle East in the last 5 Ma. This increase is more evident in areas of active tectonics and/or high topographic relief. Although we cannot exclude a tectonic contribution to some of these higher rates, the occurrence of higher exhumation rates, even in regions that did not experience enhanced tectonic activity, indicates that such an increase occurred most likely in response to the late Cenozoic global cooling and the Pleistocene increase in climate cyclicity.

1. Introduction

The diachronous opening of the western Neo-Tethys ocean and associated branches (i.e., the Alpine Tethys, and the Vardar and the Pindos Oceans among others) and its subsequent diachronous and incomplete closure through a series of Cenozoic subduction zones and collisional events, has produced a complex mosaic of deformed crustal domains including mountain belts and foreland, back-arc, strike-slip and intermontane sedimentary basins (Figs. 1 and 2; Carminati et al., 2012, 2013; Jolivet and Faccenna, 2000; Malinverno and Ryan, 1986; Royden and Faccenna, 2018). Premiere examples of these highly dynamic systems are represented by the peri-Mediterranean orogenic belts (e.g., Hellenides, Dinarides, Carpathians, Alps, Apennines, Pyrenees, Betics, Rif, Atlas) and back-arc domains (e.g., Pannonian, Aegean, Tyrrhenian, Liguro-Provencal and Alboran), which developed within the Africa-Europe convergent plate boundary zone (Faccenna et al., 2014; Jolivet and Brun, 2010; Jolivet and Faccenna, 2000; Royden, 1993). At the same time, the complete subduction of the Tethyan oceanic lithosphere

* Corresponding author at: Department of Earth Sciences, University of Florence, Italy.
E-mail addresses: riccardo.lanari@unifi.it (R. Lanari), claudio.faccenna@uniroma3.it (C. Faccenna), frederic.herman@unil.ch (F. Herman), swillett@erdw.ethz.ch (S.D. Willett), paolo.ballato@uniroma3.it (P. Ballato).

https://doi.org/10.1016/j.earscirev.2023.104328
Received 20 June 2022; Received in revised form 15 January 2023; Accepted 17 January 2023
Available online 20 January 2023

and the collision between Arabia and Eurasia in the Middle East led to the development of a wide, subaerial, convergent plate boundary that includes orogenic plateaus (e.g., Anatolian and Iranian plateaus) and mountain belts (e.g., Zagros, Alborz, Talesh, Bitlis, Caucasus, Pontides, Torides) of different size and elevation (e.g. Agard et al., 2011; Ballato et al., 2011; Mouthereau, 2011; Okay, 2008).

This complex and diverse convergent plate boundary has been investigated for over a century (e.g., Argand 1916), although the timing and the causal relationships among different orogenic events has been matter of debate. The advent of low-temperature thermochronology changed the picture by allowing the determination of rock cooling ages across a broad temperature window characteristic of the upper 10 km of the crust (e.g. Ehlers and Farley, 2003; Gallagher et al., 2005; Reiners and Brandon, 2006; Seward and Mancktelow, 1994; Wagner, 1979). Low-temperature thermochronology provides cooling ages that can be converted in exhumation rates assuming a geothermal gradient. Furthermore, the coupling of thermochronological data with stratigraphic, structural, and geomorphological data provides constraints on the principal factors controlling the cooling history and the geological evolution of specific areas. This includes timing, rates, and spatio-temporal patterns of tectonic denudation, which can exceed erosion during normal faulting, and of erosion associated with the generation of topographic relief at all scales through tectonic uplift(Fig. 2).

Over the last few decades many studies dealt with the exhumation history of mountain belts and extensional domains formed during the diachronous closure of the Tethyan ocean (e.g. Ballato et al., 2018; Erlanger et al., 2022; Fitzgerald et al., 1999; Fox et al., 2016; Lanari et al., 2020b; Ring and Layer, 2003; Schlunegger and Willett, 1999; Seward and Mancktelow, 1994; Thomson et al., 2010; Vernon et al., 2008). These studies, and many others, have provided constraints on the timing of activity of specific structures and the magnitude of associated exhumation. Thermochronometric studies are often local in spatial scale to assess and interpret mechanisms and patterns of exhumation. The patchwork nature of local studies makes it difficult to recognize regional patterns of events and the relative sequence, synchronicity, or possible teleconnections between tectonic and erosional events. For example, simultaneous changes in exhumation rates across different tectonic domains may reflect changes in the plate boundary conditions or prove the existence of unrecognized structural connections among different domains (e.g. Jolivet and Faccenna, 2000). Furthermore, a widespread increase in exhumation rates without a major increase in convergence rates for specific time windows may reflect the occurrence of more intense erosive conditions associated with climate changes (e.g. Herman et al., 2013; Molnar, 2004; Willett, 2010).

In this paper, we conduct a review analysis of thermochronometric ages across the full Mediterranean-Middle East region from Iran to Iberia and Morocco. We combine cooling ages from different thermochronometric systems using a nested approach in which data are analyzed within 19 isolated and independent tectonic provinces using a common methodology to resolve cooling histories in a common format of 5 Ma timesteps from 65 Ma to the present. Thermochronometric ages within each province are statistically combined through a formal data inversion method, thereby providing an optimal exhumation model, and importantly, an estimate of the associated resolution of the exhumation provided by the specific age distributions (Fox et al., 2014; Willett et al., 2021). These regional studies are integrated by combining and visualizing them within a plate tectonic reconstruction built with the GPlates software. This effort represents the first comparative study of timing and rates of exhumation for the entire Cenozoic in the Mediterranean and Middle East, permitting a more comprehensive interpretation in terms of tectonic events and associated erosion patterns.

1.1. *Tectonic background of the Mediterranean- Middle East*

The evolution of the Mediterranean and the Middle East is related to the subduction of the Tethyan ocean and accretion of Gondwana-derived micro-plates, such as Adria, Apulia and Arabia, onto the southern margin of the Eurasian plate (e.g. Dewey and Şengör, 1979; Şengör, 1984; Stampfli and Borel, 2002; van Hinsbergen et al., 2020). Traces of the ancient ocean are attested to by ophiolitic sutures as well as structural reconstructions, provenance studies and kinematic indicators (Fig. 1).

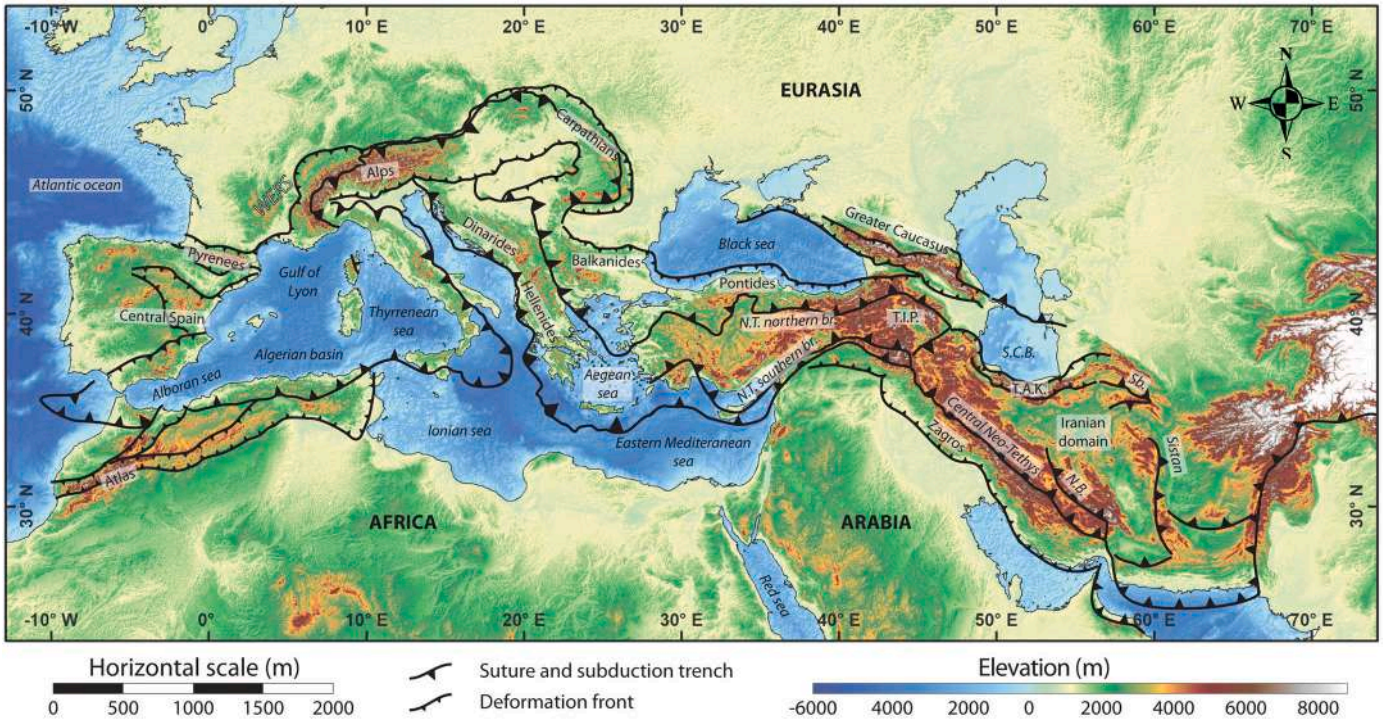

Fig. 1. Simplified tectonic map of the Mediterranean and Middle East area showing the main Neo-Tethys ophiolitic sutures and the main tectonic structures. Elevation values are extracted from the ETOPO1 DEM (Amante and Eakins, 2009).

The Neo-Tethys ocean formed during the Triassic to early Jurassic when the Iranian domain drifted northward and collided with the southern Eurasian margin leading to the demise of the Paleo-Tethys ocean (Şengör, 1984; Zanchi et al., 2009). The oceanic crust located south of the Makran accretionary wedge is considered the last remnant of the Central Neo-Tethys ocean (Barrier and Vrielynck, 2008). The demise of the Neo-Tethys northern branch throughout the Mesozoic is attested to by Triassic to Cretaceous ophiolitic mélanges found in the Pontic area (e.g. Okay, 2008). The NW continuation of the northern Neo-Tethys branch, the Vardar ocean, was consumed from the late Cretaceous to the early Paleogene leading to the collision of Adria with the southern Eurasian margin (Schmid et al., 2008). The southern branch of the Neo-Tethys was located south of the eastern Anatolian terrane and north of the Arabian plate and was opened during the early Mesozoic detachment of Anatolia from the Gondwana plate (Barrier and Vrielynck, 2008; Rolland et al., 2012; Şengör, 1984). This branch of the Neo-Tethys started to subduct northward during the late Cretaceous following the accretion of the Anatolian terrane onto the southern margin of Eurasia (~70 Ma, e.g. Rolland et al., 2012). Its final closure and the consequent Arabia-Eurasia collision occurred between the late Eocene and the early Oligocene possibly within a south-eastward younging trend (Darin and Umhoefer, 2022; McQuarrie and van Hinsbergen, 2013). To the north and west, the Liguro-Piemont basin separated the Apulian from the Eurasian plate during the opening of the central Atlantic oceanic basin (e.g. Frizon de Lamotte et al., 2009; Handy et al., 2010; Jolivet and Faccenna, 2000; van Hinsbergen et al., 2020). Its western part was mostly consumed by subduction of the Calabrian and Hellenic slabs and the coeval opening of the Liguro-Provençal, Tyrrhenian Sea and Aegean back-arcs (Carminati et al., 2012; Doglioni et al., 2002; Gueguen et al., 1998; Jolivet and Faccenna, 2000). During the Neogene, the north-westward motion of Africa produced the compressional inversion of the southern margins of the western Mediterranean back-arc basins, from Gibraltar to Sicily (e.g. Billi et al., 2011).

2. Methods

2.1. Thermochronometric data compilation

In this study we have compiled >7300 low-temperature thermochronological ages. Apatite and zircon fission track ages (AFT and ZFT, respectively) and apatite and zircon (U-Th-Sm)/He ages (AH and ZHe, respectively) and their associated errors were complied in a database including sample name, coordinates, altitude, and publication reference (see Supplementary Material 1). For several data, the sample elevations were not available, thus we extracted them from the DTM ETOPO1 (Amante and Eakins, 2009). The compiled thermochronological ages range from Proterozoic to Quaternary. However, we considered only ages younger than 70 Ma because our focus is on the Cenozoic history and the collision of the Arabian and African plates with the Eurasian plate. Furthermore, we excluded thermochronological ages from magmatic and volcanic deposits reflecting magmatic cooling instead of exhumation (e.g. Malusà et al., 2011), and thermochronological ages from sedimentary rocks where the cooling age was older than the stratigraphic age as these retains a detrital signal and hence are partially reset to unreset (e.g. Rahl et al., 2007). The final compilation after this filtering is presented in Figs. 3 and 4.

Data were organized into 19 tectonic regions (Fig. 4), defined and delimited by major tectonic structures, relatively homogenous crustal thickness and characteristics (e.g., Faccenna and Becker, 2020; Gvirtzman et al., 2016), and possibly heat flow homogeneity (Davies, 2013). According to these criteria, each region should be characterized by a relatively homogenous tectono-sedimentary and tectono-magmatic history. We will refer to these regions as blocks, although it should be

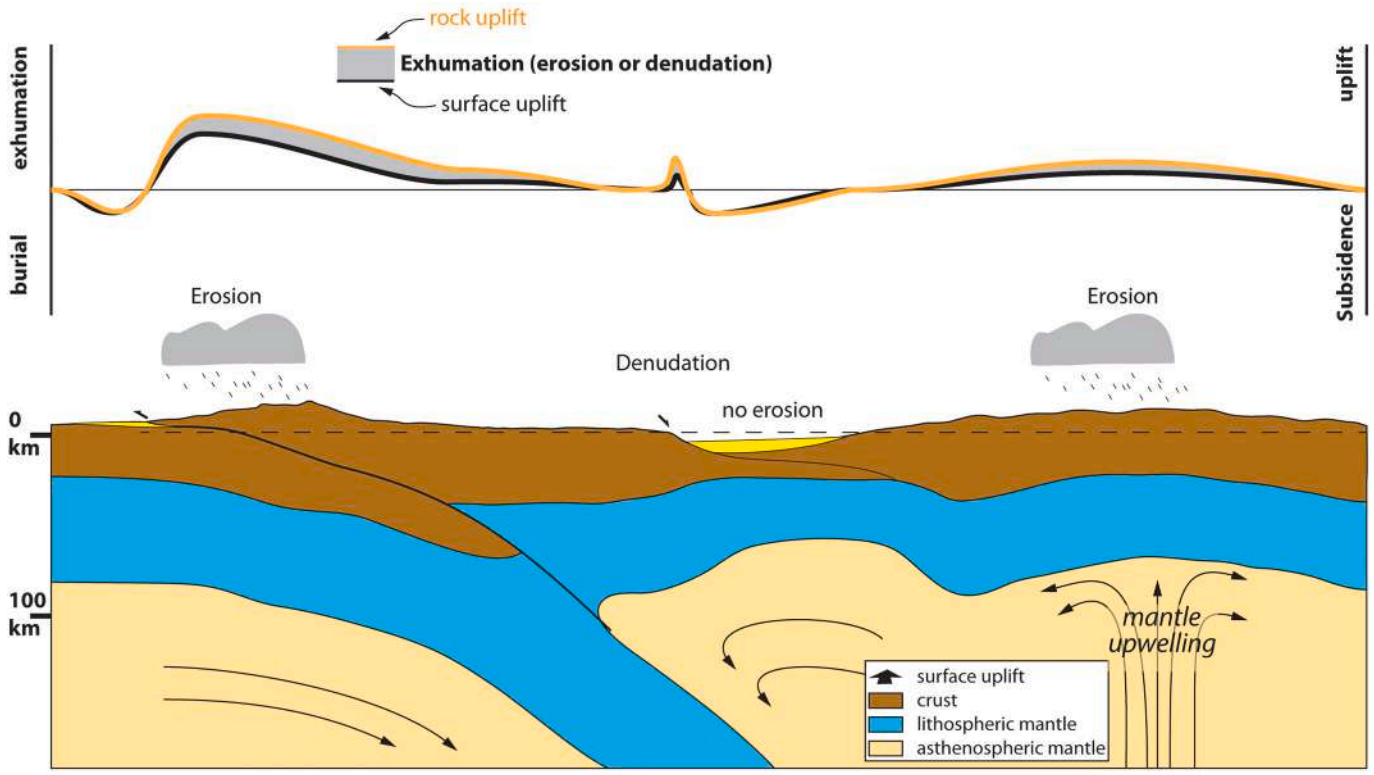

Fig. 2. Conceptual sketch showing different exhumation processes. From left to right: surface erosion induced by crustal thickening, tectonic denudation, and large wavelength erosion induced by mantle upwelling.

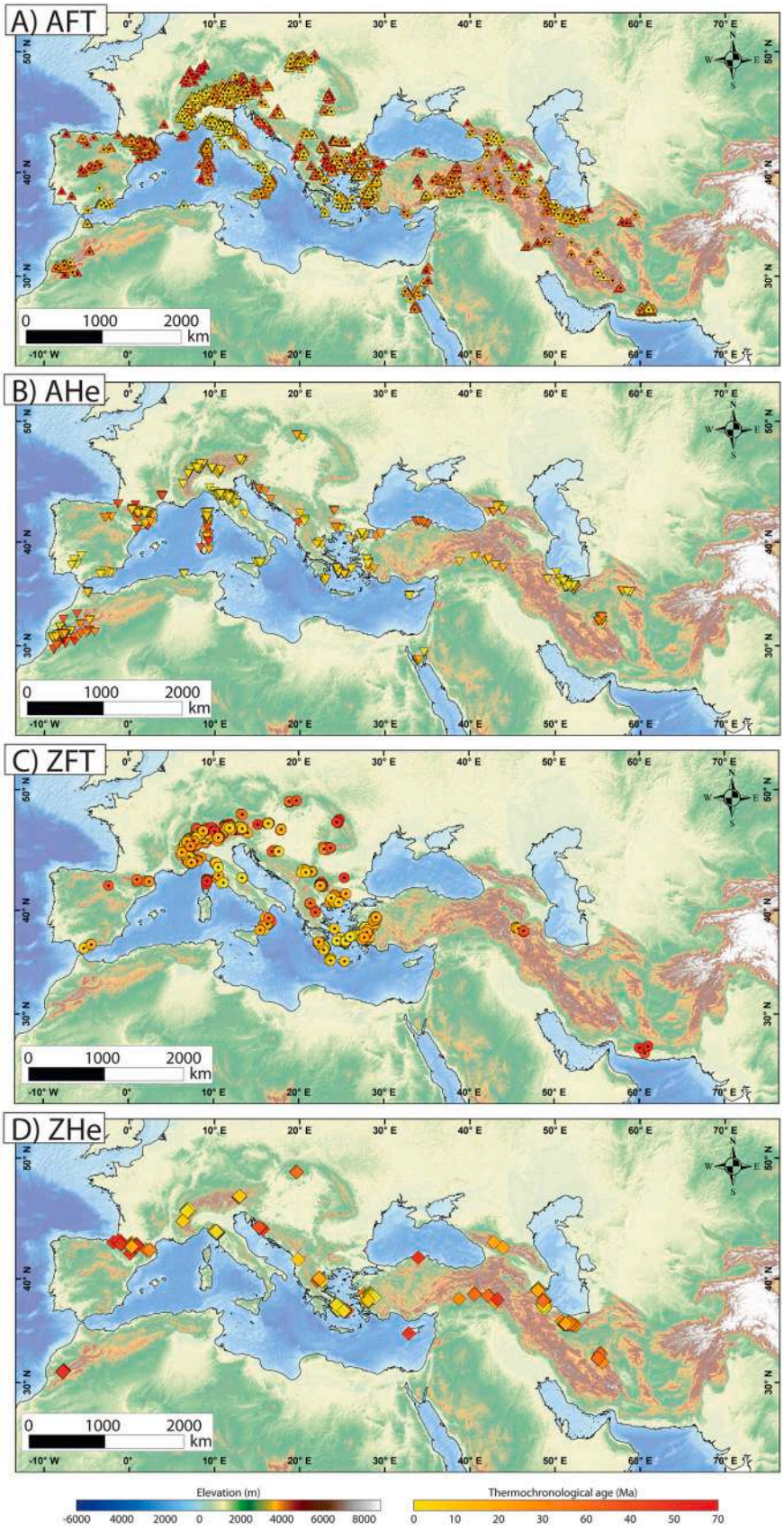

Fig. 3. Location and values of the low-temperature thermochronological AFT, AHe, ZFT, and ZHe ages in the studied area. Only data younger than 70 Ma from non-volcanic/volcaniclastic deposits samples are inverted for exhumation rates (see details in the text). Range of ages for each region and each thermochronometers are shown in the histograms in Fig. 4.

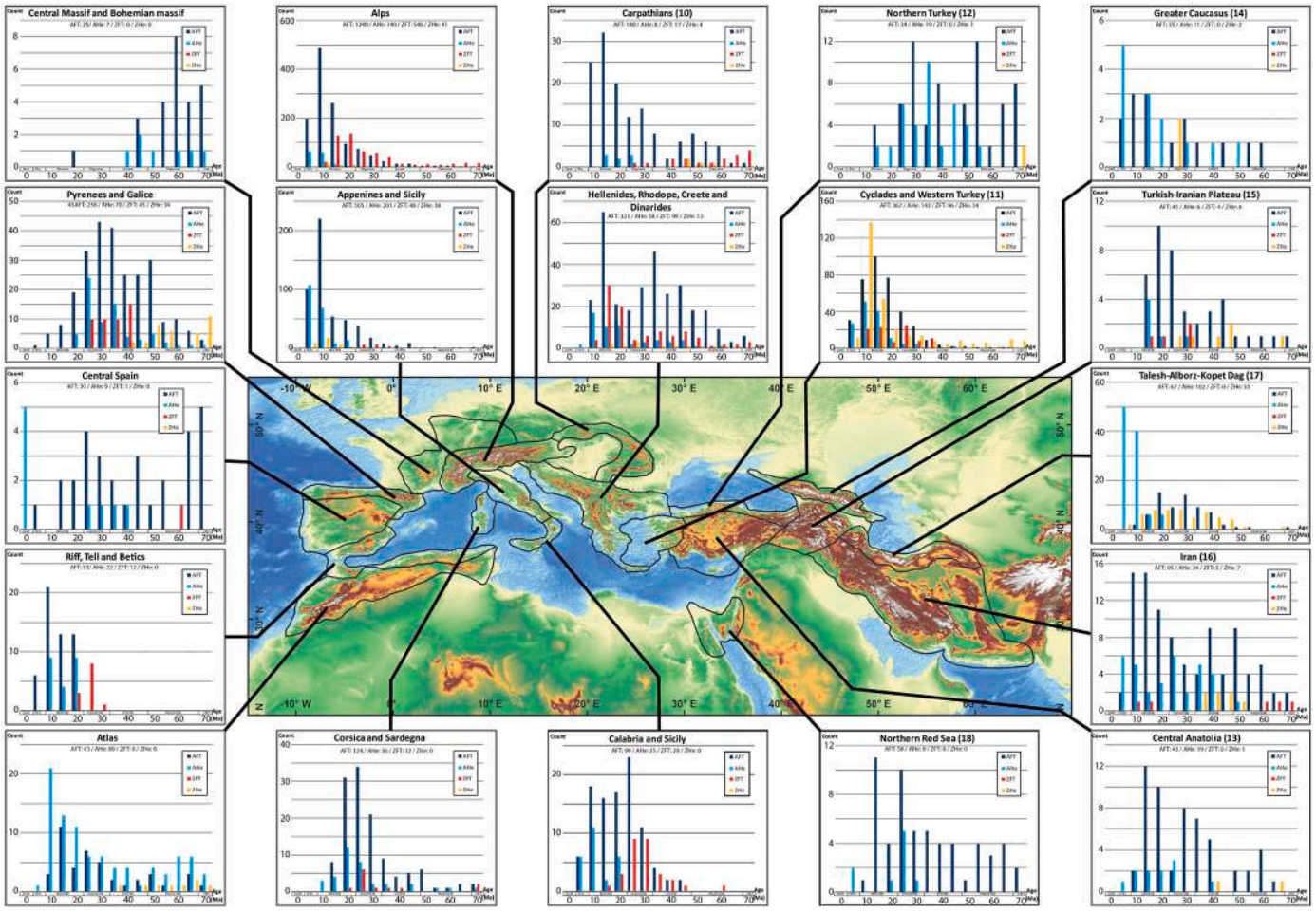

Fig. 4. Low-temperature thermochronological data used for the thermal inversion and presented in Fig. 3. Data were assembled into 19 tectonically areas, following the main structural elements, the crustal thickness, and heat flow patterns.

noted that this does not imply that these blocks represent rigid structural elements. The distribution of the compiled ages within each block for each thermochronometer is shown in Fig. 4.

Overall, we defined five tectonic blocks in the Middle East: the Iranian domain, the Talesh-Alborz-Kopeh Dagh (TAK), the Turkish-Iranian Plateau, the Greater Caucasus, and the Northern Red Sea. In the eastern Mediterranean area, we defined six blocks, the Central Anatolia, the Pontides, the Aegean-Western Anatolia, the Dinarides-Hellenides, the Carpathians, and the Alps. In the Western Mediterranean area, we defined regions corresponding to the Pyrenees, the Iberian range, and the Corsica-Sardinia blocks. For the Italian peninsula, we separated the Apennines from the Calabria-Sicily block, because of their differential south-eastward motion associated with slab roll-back. South of the Iberian plate, we defined the Rif-Tell-Betics and the Atlas blocks. The Central and the Bohemian massifs were considered a single block.

2.2. Tectonic reconstruction

To place the cooling ages and associated erosion rates into the evolving geodynamic context we built a tectonic reconstruction using the GPlates software (Müller et al., 2008) and incorporated plate velocities from Seton et al. (2012a) and Müller et al. (2008) as kinematic constraints at the boundaries. The model integrates different data from multiple studies. Specifically, the motion and shape of the individual blocks in the Middle East is based on the ophiolitic suture geometry and the reconstructions of Barrier and Vrielynck (2008), Rolland et al. (2012), Rolland (2017), van Hinsbergen et al. (2020) and Boutoux et al. (2021). For the eastern Mediterranean we used the reconstructions of Jolivet and Faccenna (2000), Barrier and Vrielynck (2008), Jolivet et al. (2013), Menant et al. (2016), and van Hinsbergen et al. (2020). Finally, the motions of the tectonic blocks in the central and western Mediterranean area are based on Jolivet and Faccenna (2000), Faccenna et al. (2004 and 2014); Frizon de Lamotte et al. (2009), Royden and Faccenna (2018) and van Hinsbergen et al. (2020). Trench positions back in time were reconstructed by subtracting the oceanic-floored area of each basin and then, using an area balancing technique, by restoring the crust to the thickness of the surrounding undeformed continental domains (typically 30 km). We considered the simplest setting even for regions where recent reconstructions suggested the occurrence of hyper-extended continental domains rather than oceanic crust (see for example the Western Mediterranean, Romagny et al., 2020; Angrand and Mouthereau, 2021; Vergés and Fernàndez, 2012). We used information on width and thickness of the former passive margins along the Tethys, allowing estimation of extension in addition to spreading magnitudes. Subduction velocities have been estimated by adding the velocity of convergence of the downgoing plate, taken perpendicular to the subduction zone, to the trench retreat. In our tectonic reconstruction, we defined the transition between shallow and deep marine environment at the 600 m deep isobath. This value corresponds to the uppermost part of the continental shelf, and to a first approximation it could be considered as the transition from continental to oceanic lithospheric domains (Fig. 5).

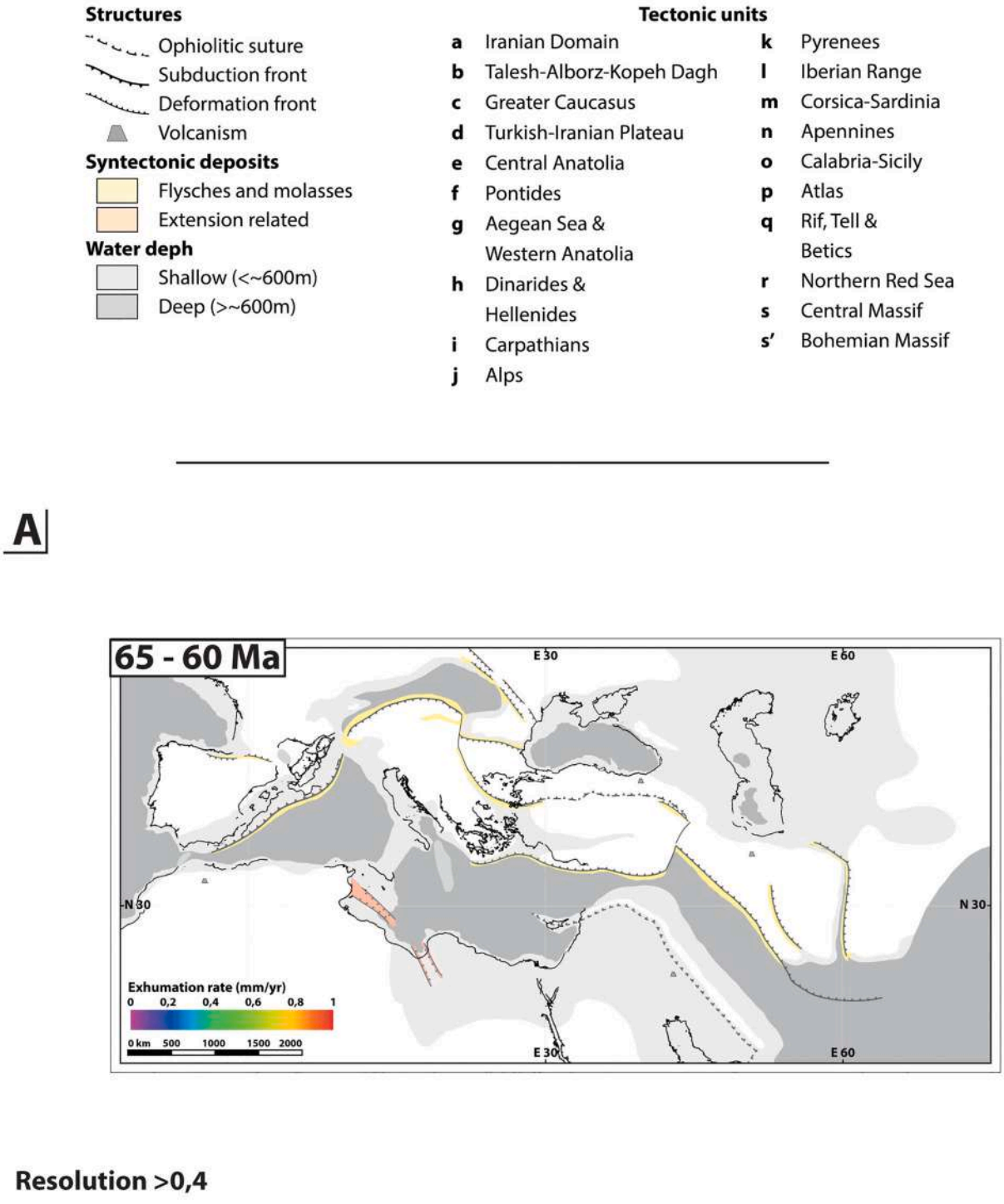

Fig. 5. Inferred Cenozoic exhumation rates on our plate tectonic reconstruction. Low-temperature thermochronological data were inverted with Glide thermal model and computed separately for each of the 19 tectonic blocks. Exhumation rates at each time step are indicated by color on the map and the range of values for each region is shown in the histograms. Results are shown only for rates with a temporal resolution above 0.4 (results for different resolution are available within the supplementary material).

2.3. Forward and inverse thermal modeling

Thermochronometric ages are converted to exhumation rates through a thermal model. Thermal processes in the near surface environment that are potentially important include upward advection by erosion, 3-D structure in the temperature field due to surface topography, and advection of heat by tectonic motion and there are published models designed to deal with these effects (Braun, 2002, 2003; Fox et al., 2014; Willett and Brandon, 2013). Thermal models must be combined with a prediction of age that follows temperature-dependent kinetic behavior for loss of radioactive decay products. The simplest form of a daughter loss model is that of a closure temperature, which defines the temperature corresponding to the measured age, assuming a constant rate of cooling (Dodson, 1973).

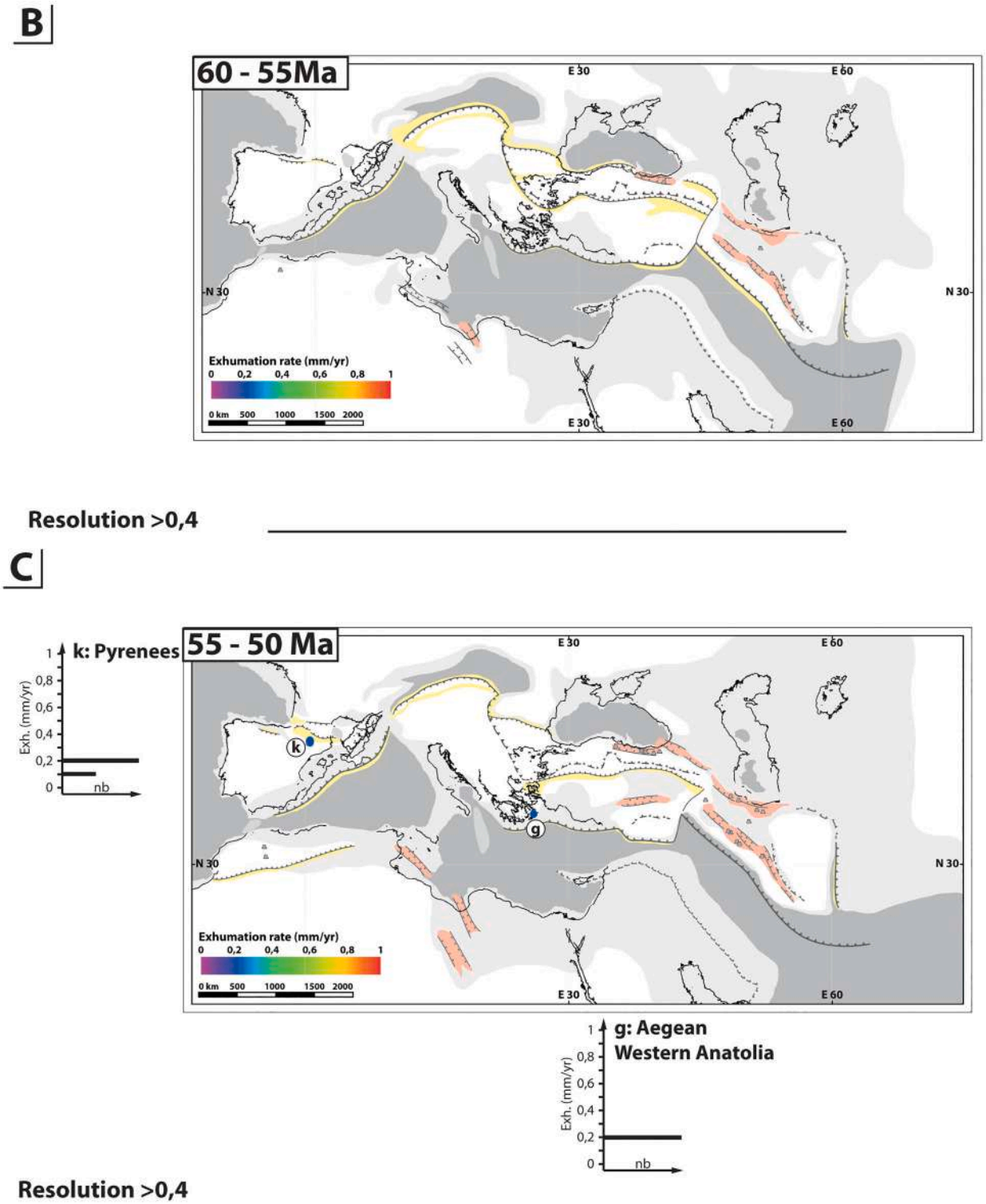

Fig. 5. (*continued*).

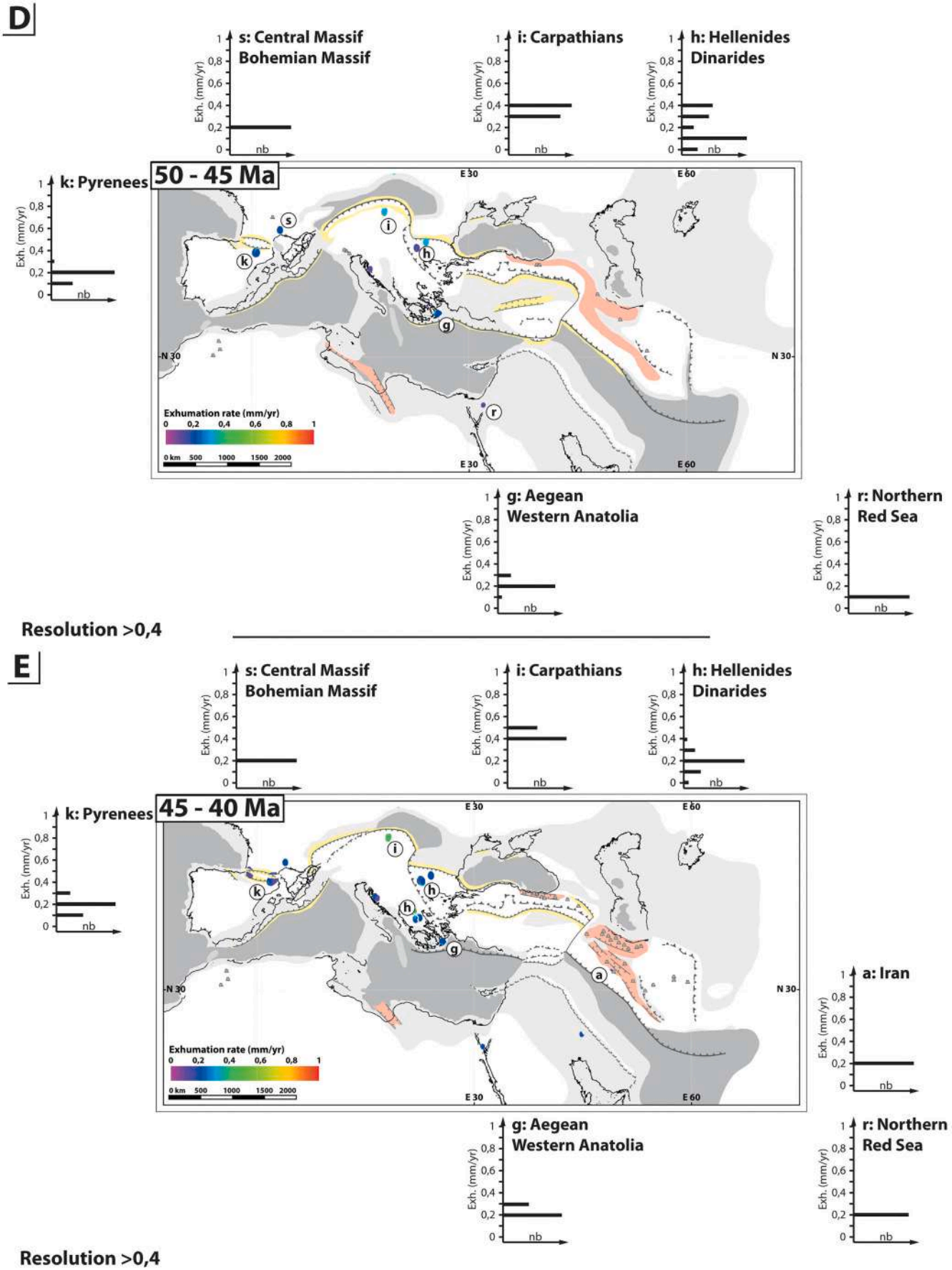

Fig. 5. (*continued*).

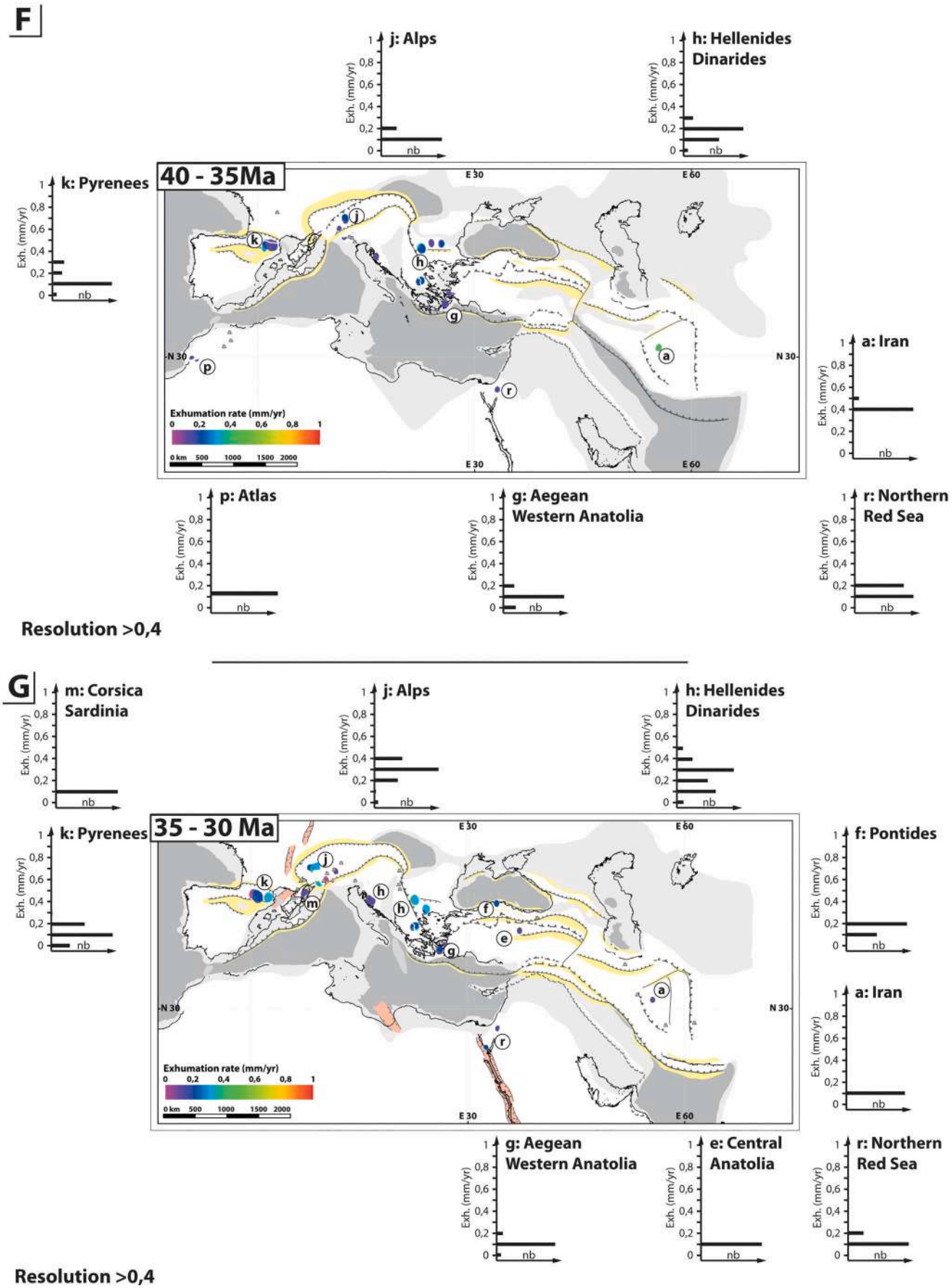

Fig. 5. (*continued*).

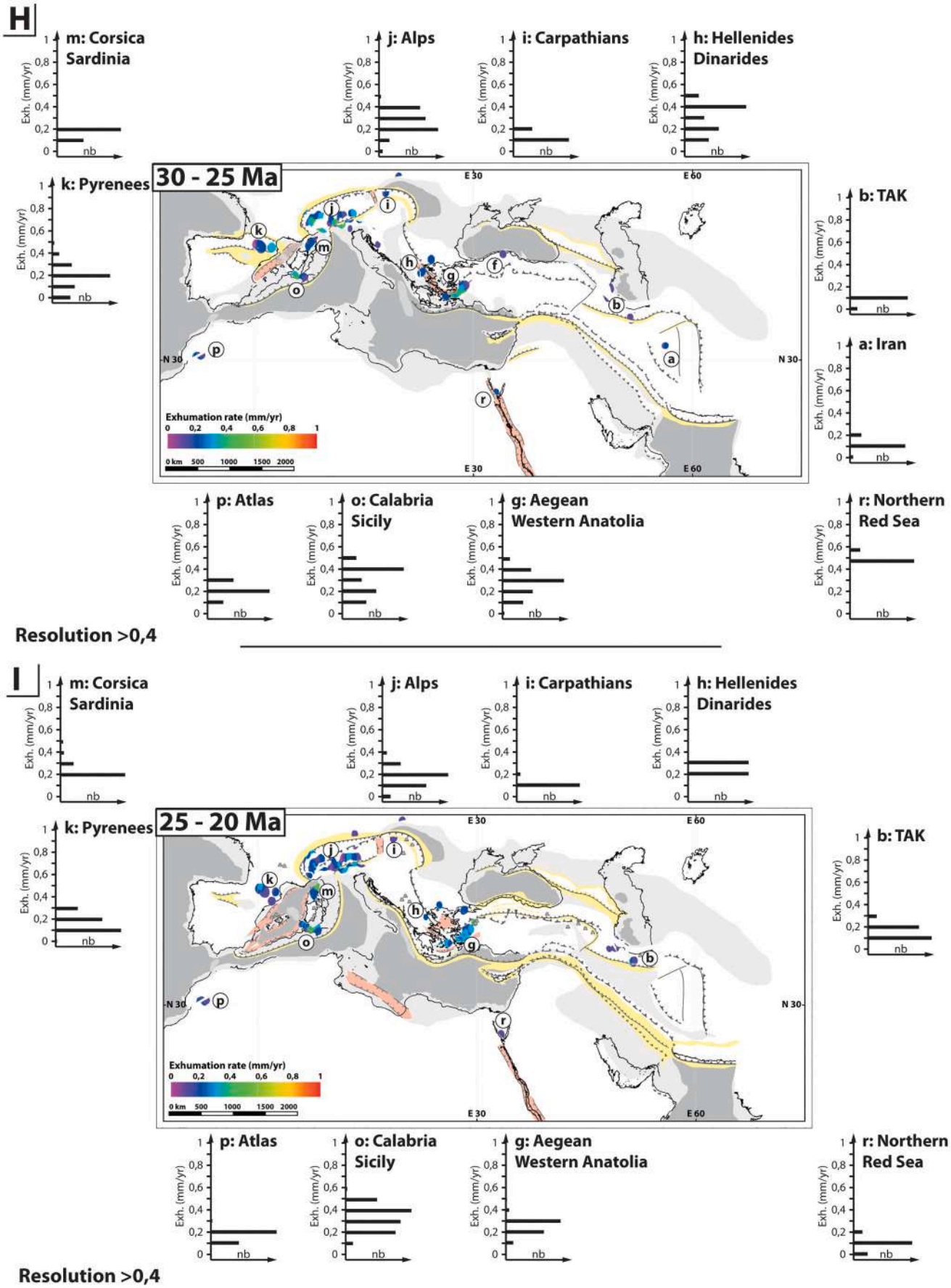

Fig. 5. (*continued*).

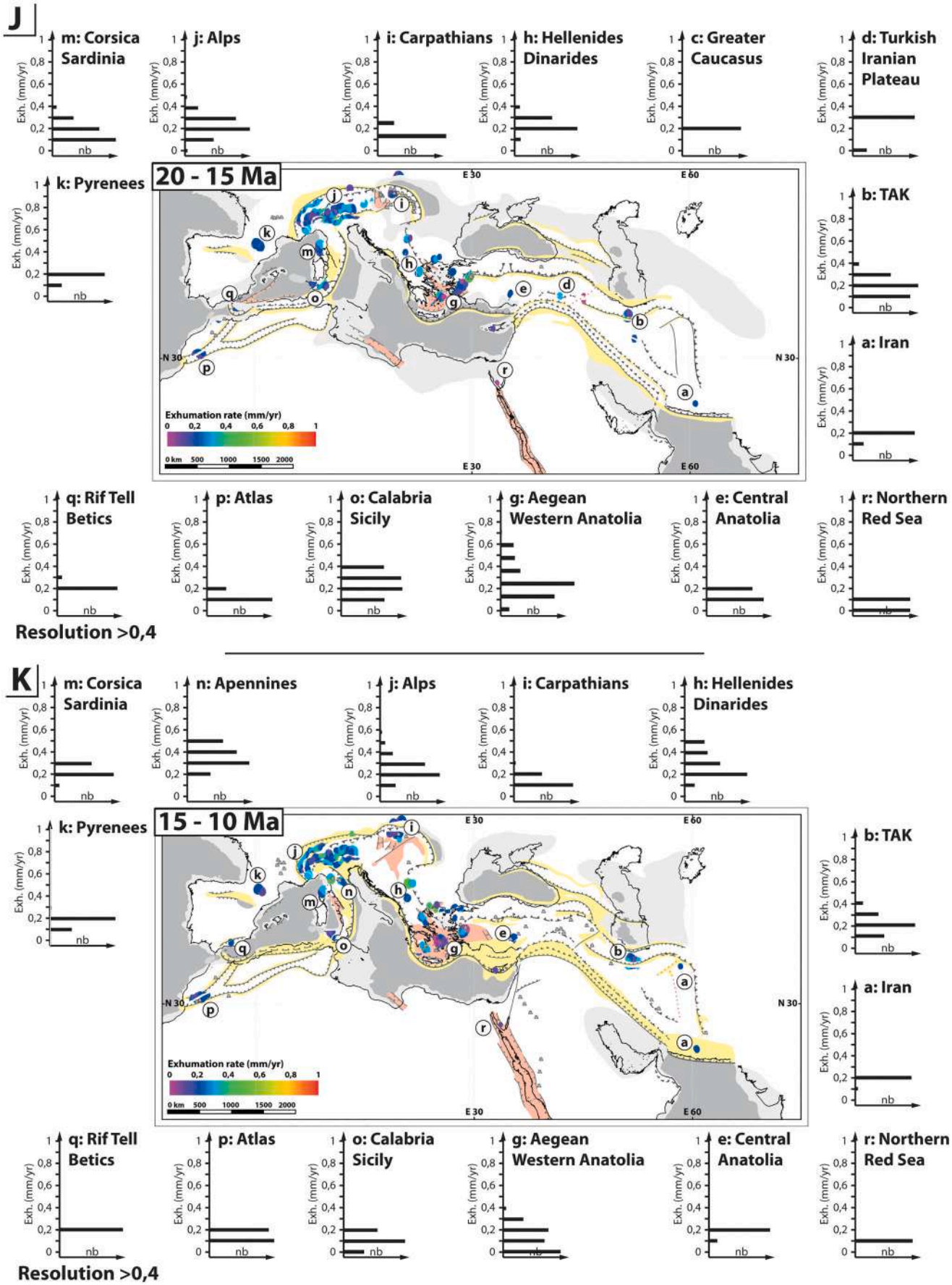

Fig. 5. (*continued*).

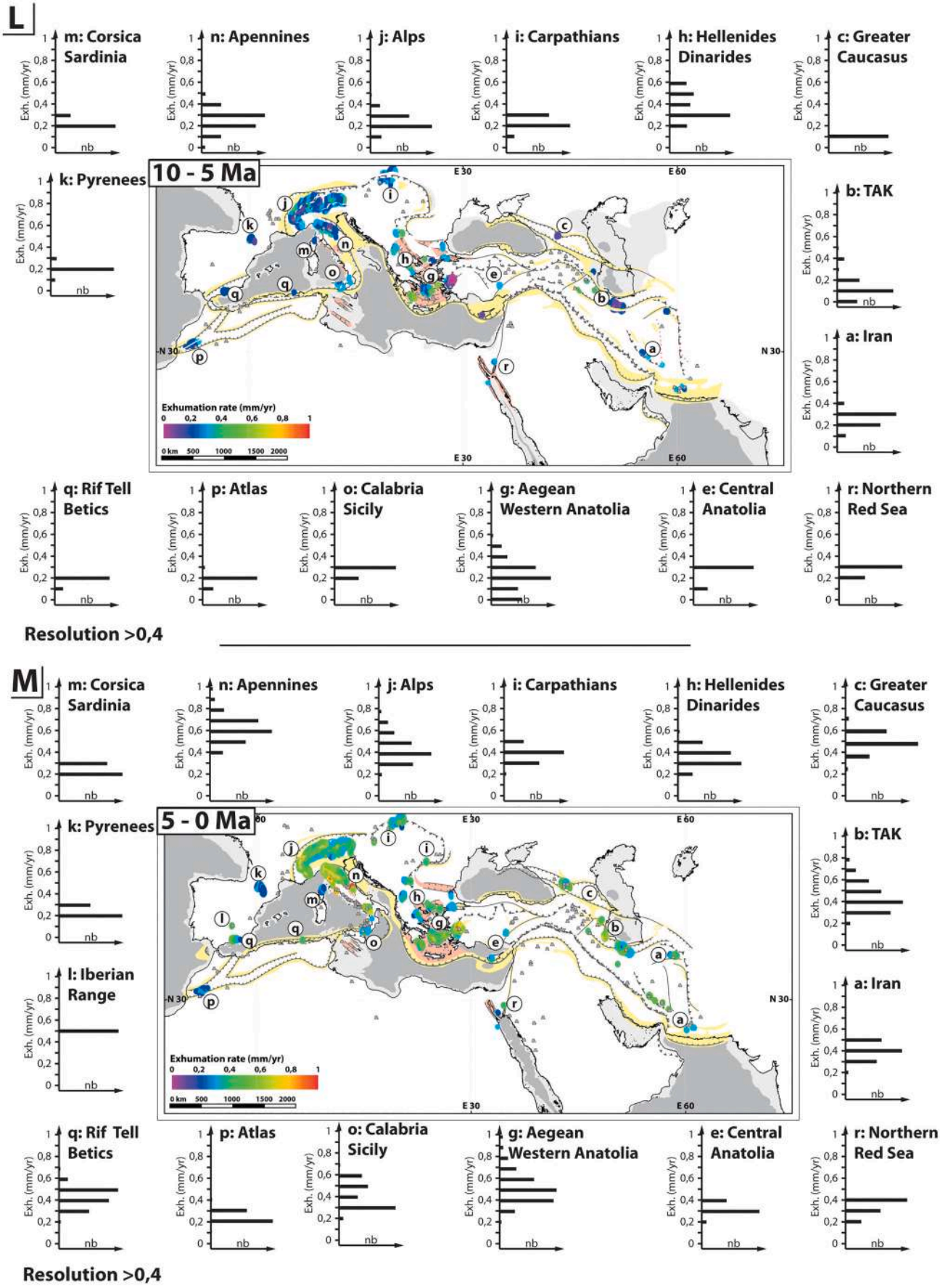

Fig. 5. (*continued*).

In this paper, we use the inversion method of Fox et al. (2014), further developed by Jiao et al. (2017) and Willett et al. (2021). This inversion approach uses the closure depth concept and calculates the depth to closure isotherms using a thermal model including the effects of topography of the upper surface and advection of heat by the upward motion of rock during exhumation (Fox et al., 2014). The depth to the closure isotherm is calculated in one dimension, but lateral erosion rates are forced to be smooth through a spatial correlation function. This correlation structure is imbedded in a Bayesian inverse method with a prior and posterior covariance structure, so that the estimate of the exhumation rates is:

$$\boldsymbol{e}_{post} = \boldsymbol{e}_{prior} + \left(\mathbf{C}\mathbf{A}^{t}\left(\mathbf{A}\mathbf{C}\mathbf{A}^{t} + \mathbf{C}_{\epsilon}\right)^{-1}\right)\left(\mathbf{z}_{c} - \mathbf{A}\boldsymbol{e}_{prior}\right) \quad (1)$$

where **A** is a matrix that includes the ages divided into timesteps, **C** is the prior covariance matrix, or model covariance, $\mathbf{C}_{\epsilon}$ is the data covariance (which is a diagonal matrix that includes the error on the closure depths), $\mathbf{z}_{c}$ is a vector of the sample closure depths, $\boldsymbol{e}_{prior}$ is a vector that represents the prior exhumation rate (i.e., some prior guess of the exhumation rates before solving Eq. 1), $\boldsymbol{e}_{post}$ is the inferred exhumation rates, which is a vector of estimated exhumation rate at each data location. Ages are converted to a depth, z_c, using the imbedded thermal model.

From Eq. 1, one can define the inverse operator, **H,** as

$$\mathbf{H} = \mathbf{C}\mathbf{A}^{t}\left(\mathbf{A}\mathbf{C}\mathbf{A}^{t} + \mathbf{C}_{\epsilon}\right)^{-1} \quad (2)$$

and each element of **C** is given by

$$C(\mathrm{I},\mathrm{j}) = \sigma^{2} exp\left(-\frac{d^{2}}{L^{2}}\right) \quad (3)$$

where σ^2, L and d are the prior variance, a correlation length scale and the separation distance between samples, respectively.

Note that the goal of Eq. 1 is to minimize an objective function given by

$$2S(\boldsymbol{e}) = (\mathbf{z}_{\mathbf{m}} - \mathbf{z}_{\mathbf{c}})^{t}\mathbf{C}_{\epsilon}^{-1}(\mathbf{z}_{\mathbf{m}} - \mathbf{z}_{\mathbf{c}}) + \left(\boldsymbol{e} - \boldsymbol{e}_{prior}\right)^{t}\mathbf{C}^{-1}\left(\boldsymbol{e} - \boldsymbol{e}_{prior}\right) \quad (4)$$

To assess the inversion results, Fox et al. (2014) proposed to analyze the posterior variance and the resolution. The posterior covariance matrix is given by

$$\mathbf{C}_{post} = \mathbf{C} - \mathbf{H}\mathbf{A}\mathbf{C} \quad (5)$$

and the resolution, **R**, can be computed as follows.

$$\mathbf{R} = \mathrm{HA} \quad (6)$$

and provides a means to evaluate whether the exhumation rates are resolved or not (Tarantola, 2005; Fox et al., 2014; Willett et al., 2021).

To assess the quality of the solution we also monitor the 'reduced variance', which is the ratio between the a priori and a posteriori variance. This value is between zero and one. The closer to zero, the better the solution (Fox et al., 2014). Lower reduced variance implies that more data have been averaged for the solution, so the estimate should be more accurate, although it also implies more data averaging. All model results are combined into a single map result (Fig. 5) to illustrate the patterns at all spatio-temporal scales. This summary figure is based on our original tectonic reconstruction of the Mediterranean and Middle East areas for the Cenozoic.

Results of the thermochronometric model analysis are in form of space-time distributions of erosion rate and are shown in a series of paleo tectonic maps including the estimated exhumation rates shown in time increments of 5 Ma (Fig. 5). For each tectonic block, we extracted the exhumation rates of regions where the resolution exceeds a threshold of 0.4. Various tests were performed to establish the threshold level for reliable exhumation rates, following the discussion in Willett et al. (2021). These tests are shown in Supplementary Material 3. Similar tests were performed using differing values of the reduced variance. They are presented in Supplementary Material 4. The exhumation rates that are sufficiently resolved are presented in map view (Fig. 5) and as timelines for each region (Fig. 6). The histograms represent inferred exhumation rates for a specific block and for a peculiar time-step. In addition, in Fig. 6, for every block and every time-step, we add additional tectonic information, such as the mode of deformation (extensional or contractional). We compare our results with: 1) subduction rates (convergence velocity plus trench retreat velocity) for areas characterized by oceanic subduction and retreating tranches where exhumation is mostly related to tectonic exhumation and erosion of uplifted footwall blocks (e.g., Aegean Western Anatolia, Carpathians, Apennines, Corsica Sardinia, Calabria Sicily and Rif Tell Betics); 2) divergence rates for divergent plate boundaries (e.g., Northern Red Sea); and 3) plate convergence velocities for continental collisions and intracontinental deformation zones where exhumation is driven by relief generation and associated surface erosion (Fig. 6). In addition, since climate variations (i.e., increase in precipitation rates and in frequency of high magnitude events; establishment of glacial-interglacial cycles) are expected to affect exhumation processes enhancing surface erosion (e.g., Herman et al., 2013 and references therein), we also compare our results for each tectonic block and over each time step, with the $\delta^{18}O$ curve obtained from deep-water benthic foraminifera (Fig. 6; Zachos et al., 2008). This curve is the most representative proxy for Cenozoic global climate because it includes the most continuous record with the highest temporal resolution. Although there may be important local or regional effects on exhumation rates, the global record should capture major climate events, and permit us to identify potential common events that correlate across regions.

3. Results: Inferred exhumation rates

Inferred exhumation rates with high resolution are visualized together with our plate tectonic reconstruction in Fig. 5 and in plots where they are compared with regional tectonic rates (i.e., plate convergence or subduction or divergence rates; Fig. 6) and with the Earth temperature history as a proxy of climatic variations (Fig. 6). The contribution of each thermochronometric system for the different analyzed time steps is evident in Fig. 4. Due to the large number and appropriate age distibution, AFT cooling ages contribute more to the calculation of the high-resolution exhumation rates.

3.1. Earliest Paleocene to earliest Eocene (65–55 Ma timesteps)

Several low-temperature thermochronological data yielding ages between 70 and 55 Ma are present in our database (e.g., in the Alps, Hellenides Dinarides in the Iran tectonic blocks, Fig. 4; Fig. 5A and B). These ages, however, are too few to resolve exhumation rates over specific time intervals (i.e., with a resolution <0.4), so we do not report any rate for the earliest Cenozoic (Figs. 4, 5A and B).

3.2. Earliest Eocene to latest Eocene (55–35 Ma timesteps)

The number of low-temperature thermochronological ages compiled in the database increases significantly from the Eocene (Figs. 4 and 5C to 5F). In the Middle East (Iranian block) our inverse modeling shows well-resolved exhumation rates (i.e., with a resolution >0.4) of 0.2 mm/yr in the 40–45 Ma time window that increase to 0.4–0.5 mm/yr from 35 to 40 Ma (Fig. 6a). In the Northern Red Sea block, inferred exhumation rates increases at 50 Ma (0.1 mm/yr) and remain rather constant (0–1-0.2 mm/yr) for most of the Eocene (Fig. 6r).

In the central and western sectors of the Adrian plate, exhumation starts in the Aegean-Western Anatolia block during the 50–55 Ma timestep and are uniform for the entire Eocene. The most frequently occurring rates (i.e., modal rates) decrease from 0.2 (40–55 Ma) to 0.1 mm/yr (35–40 Ma). The Hellenides-Dinarides tectonic block present the

largest rates dispersion with values ranging from <0.1 to 0.4 mm/yr for most of the Eocene (35 to 50 Ma), while the modal rates increase progressively from 0.1 to 0.2 mm/yr (Fig. 6h). The Carpathians present also well-resolved exhumation rates of about 0.3–0.5 mm/yr but only for the 40–50 Ma time windows (modal rates 0.4 mm/yr; Fig. 6g). Instead, in the Alps, well-resolved exhumation rates of 0.1 to 0.2 mm/yr start only in the late Eocene (35–40 Ma; Fig. 6j).

In Europe, we observe exhumation rates of 0.1 mm/yr in the southern part of the Central Massif (Fig. 6s) whereas in the Central and Bohemian massif our analysis yields well-resolved rates of 0.1 mm/yr only during the middle Eocene (from 50 to 40 Ma, Figs. 5 and 6s).

In the Western Mediterranean, the Pyrenes are characterized by well-resolved exhumation rates for the entire Eocene, with maximum rates of 0.3 mm/yr and modal values of 0.2 and 0.1 mm/yr (Fig. 6k). Finally, during the late Eocene (35–40 Ma) well-resolved exhumation rates of 0.1 mm/yr are recorded also in the Atlas tectonic blocks (Fig. 6p).

3.3. Latest Eocene to early Miocene (35–20 Ma timesteps)

The high number of thermochronological data, from all the analyzed thermochronometric systems, with Oligocene ages allows the inference of well-resolved exhumation rates for several tectonic blocks (Figs. 4 and 5G to 5I). In the Middle East (Iranian tectonic block) the elevated late Eocene (35–40 Ma) exhumation rates of 0.4–0.5 mm/yr are followed by rates of 0.1–0.2 mm/yr (35–25 Ma), while the following time window (20–25 Ma) does not exhibit well-resolved rates (Fig. 6a). In the adjacent TAK block, the first well-resolved Oligocene exhumation rates of ~0.1 mm/yr occur from 25 to 30 Ma (Fig. 6b) and increase up to 0.3 mm/yr in the latest Oligocene (20–25 Ma; Fig. 6b). In the Northern Red Sea block, early Oligocene (30–35 Ma) exhumation rates of 0.1–0.2 mm/yr (Fig. 6R) increase to ~0.3 mm/yr from 25 to 30 Ma, before decreasing again to 0–0.2 mm/yr in the latest Oligocene (25–20 Ma; Fig. 6r).

In the eastern Adria domain, the Pontides and Central Anatolia present exhumation rates of 0.1–0.2 mm/yr only from 25 to 35 and 30 to 25 Ma, respectively (Fig. 6f and e). Concerning the central and western Adria domain, exhumation rates of 0.1–0.3 mm/yr (30–35 Ma) in the Aegean-Western Anatolia increase up to 0.5 mm/yr from 25 to 30 Ma and then decrease slightly (0.1–0.4 mm/yr) during the 20–25 Ma timestep (Fig. 6g). In the Dinarides-Hellenides a similar increase up to 0.5 mm/yr occur a bit earlier, in the 30–35 Ma time window, while the following steps present rates of 0.1–0.3 (20–30 Ma; Fig. 6h). A similar increase is observed in the Alps where exhumation rates of up to 0.4 mm/yr are observed for the entire Oligocene (Fig. 6j). Finally, in the Carpathian block well-resolved rates of 0.1–0.2 mm/yr occur in the 20–30 time windows (Fig. 6i). In the tectonic blocks of Western Adria (Aegean-Western Anatolia, Dinarides-Hellenides, Alps) Oligocene rates present a large dispersion while the modal rates are 0.2–0.3 mm/yr.

In the central Mediterranean region, we have well-resolved exhumation rates of 0.1–0.2 mm/yr in the Corsica-Sardinia block starting from the Oligocene (35–20 Ma; Fig. 6m). In the Calabria-Sicily block, we start also observing well-resolved exhumation rates during the Oligocene (30–20 Ma; Fig. 6m). These rates exhibit a large dispersion (0.1 to 0.5 mm/yr) and present high modal values of 0.4 mm/yr (Fig. 6m).

In the western Mediterranean region, in the Pyrenees block, exhumation rates of <0.1 to 0.2 mm/yr (30–35 Ma) increase up to 0.5 and 0.3 mm/yr in the following timesteps, with modal values of 0.2 and 0.1 mm/yr (25–30 and 20–25 Ma, respectively; Fig. 6k). Well-resolved exhumation rates of 0.1–0.3 m/yr are observed also in the Atlas block from 20 to 30 Ma (Fig. 6p).

3.4. Early Miocene to earliest Pliocene (20–5 Ma timesteps)

The abundance of thermochronological data with ages from the Miocene allows extracting well-resolved exhumation rates in all blocks except the Iberian, the Pontides, and the Central-Bohemian Massifs (Figs. 4 and 5j to 5l). In the Middle East, the Iran tectonic block is characterized by an increase in exhumation rates from 0.1 to 0.2 mm/yr (10–20 Ma timesteps; modal rate 0.2 mm/yr) to 0.1–0.4 mm/yr in the late Miocene (5–10 Ma; modal rate 0.3 mm/yr; Fig. 6a). Conversely, in the TAK block, exhumation rates increase slightly with respect to the 20–25 Ma step from 0.1 to 0.3 to 0.1–0.4 (15–20 Ma) and 0.1–0.5 (10–15 Ma; Fig. 6b), while modal rates increase progressively to 0.3 mm/yr in the 10–15 Ma timestep (Fig. 6b) The following 5–10 Ma timestep is also characterized by high dispersion (0–0.5 mm/yr) but the modal rates decrease sharply to 0.1 mm/yr (Fig. 6b). In the Greater Caucasus block, we observe well-resolved exhumation rates only during the middle (15–20 Ma) and the late Miocene (5–10 Ma), when the inferred rates are 0.2 mm/yr and 0.1 mm/yr respectively (Fig. 6c). In the Turkish Iranian plateau block, our model provides exhumation rates (0 and 0.3 mm/yr) only for the middle Miocene (15–20 Ma; Fig. 6d). Finally, in the Northern Red Sea block, exhumation rates increase from 0.1 mm/yr in the 10–20 Ma timesteps to 0.2–0.3 mm/yr in the late Miocene (5–10 Ma; Fig. 6r).

In the eastern Adria domain, our modeling records well-resolved exhumation rates of 0.1 to 0.2 mm/yr for the central Anatolian block from 10 to 20 Ma (for the 10–20 Ma timesteps) with an increase up to 0.3 mm/yr for the late Miocene (5–10 Ma; Fig. 6e). In the central and western Adriatic plate boundary, the Aegean-Western Anatolia block presents highly dispersed exhumation rates ranging from <0.1 to 0.5 (20−10), 0.4 (10–15 Ma), and 0.6 (5–10 Ma) mm/yr with modal values of 0.2 mm/yr except for the 10–15 Ma time window where they decrease to 0.1 mm/yr (Fig. 6g). The Hellenides-Dinaride block is also characterized by high dispersion with a progressive increase in maximum (0.4 to 0.7 mm/yr) and modal (0.2 to 0.3 mm/yr) rates from 20 to 5 Ma (Fig. 6h). In the Carpathians block the Miocene rates are similar to the Oligocene. Overall, our data show a pattern similar to the one observed in the Hellenides-Dinaride block with a slight increase in exhumation variance (0.1–0.2 to 0.1–0.3 mm/yr) and modal rates (0.1 to 0.2 mm/yr) rates from 10 to 20 Ma to 5–10 Ma (Fig. 6h). In the Alpine block, we still observe an elevated, but uniform, dispersion (as in the Oligocene) with exhumation rates ranging from <0.1 to 0.5–0.6 with modal values of 0.2 mm/yr (Fig. 6j).

In the central Mediterranean, the Corsica-Sardinia block presents a rate dispersion diminishing progressively throughout the Miocene from 0.1 to 0.4 mm/yr in the 15–20 Ma timestep to 0.2–0.3 mm/yr in the 5–10 Ma time window, while the modal values increase from 0.1 to 0.2 mm/yr (Fig. 6m). In the Apennines tectonic block, we observe well-resolved exhumation rates starting from the middle Miocene with values of 0.2–0.5 and < 0.1–0.5 for the 10–15 and 5–10 Ma time interval respectively, and modal values of 0.3 mm/yr (Fig. 6n). In the Calabria-Sicily block the 15–20 Ma exhumation rates are quite similar to the 20–30 Ma rates (0.1 to 0.4 mm/y). In the middle Miocene (10–15 Ma), the distribution tightens and rates decrease to less than <0.1–0.2 mm/yr, before increasing again at the end of the Miocene (0.2–0.3 mm/yr; Fig. 6o).

In the Pyrenees tectonic block (western Mediterranean), our inferred exhumation rates decrease slightly with respect to the Oligocene ones but stay uniform until 10 Ma (0.1–02 mm/yr, 10–20 Ma; Fig. 6k). In the late Miocene (5–10 Ma), rates increase slightly (0.1–0.3 mm/yr) although the mode remains constant (0.2 mm/yr; (Fig. 6k). In the Atlas block, exhumation rates are like the Oligocene rates (0.1 to 0.2 mm/yr until 10 Ma and 0.1 to 0.3 from 5 to 10 Ma). Modal values, instead, decrease from 0.2 to 0.1 at 20 Ma, and then increase again in the 5–10 Ma timestep (Fig. 6p). Exhumation in the Miocene starts also in the Rif Tell Betics block with values of about 0.2 mm/yr from 20 to 5 Ma (Fig. 6q).

3.5. Pliocene-Quaternary (5–0 Ma)

An increase in the inferred exhumation rates occurs in the Pliocene-Quaternary across most of the region from Iberia to the Middle East (compare Fig. 5L with 5 M and see Fig. 6). Specifically, maximum and

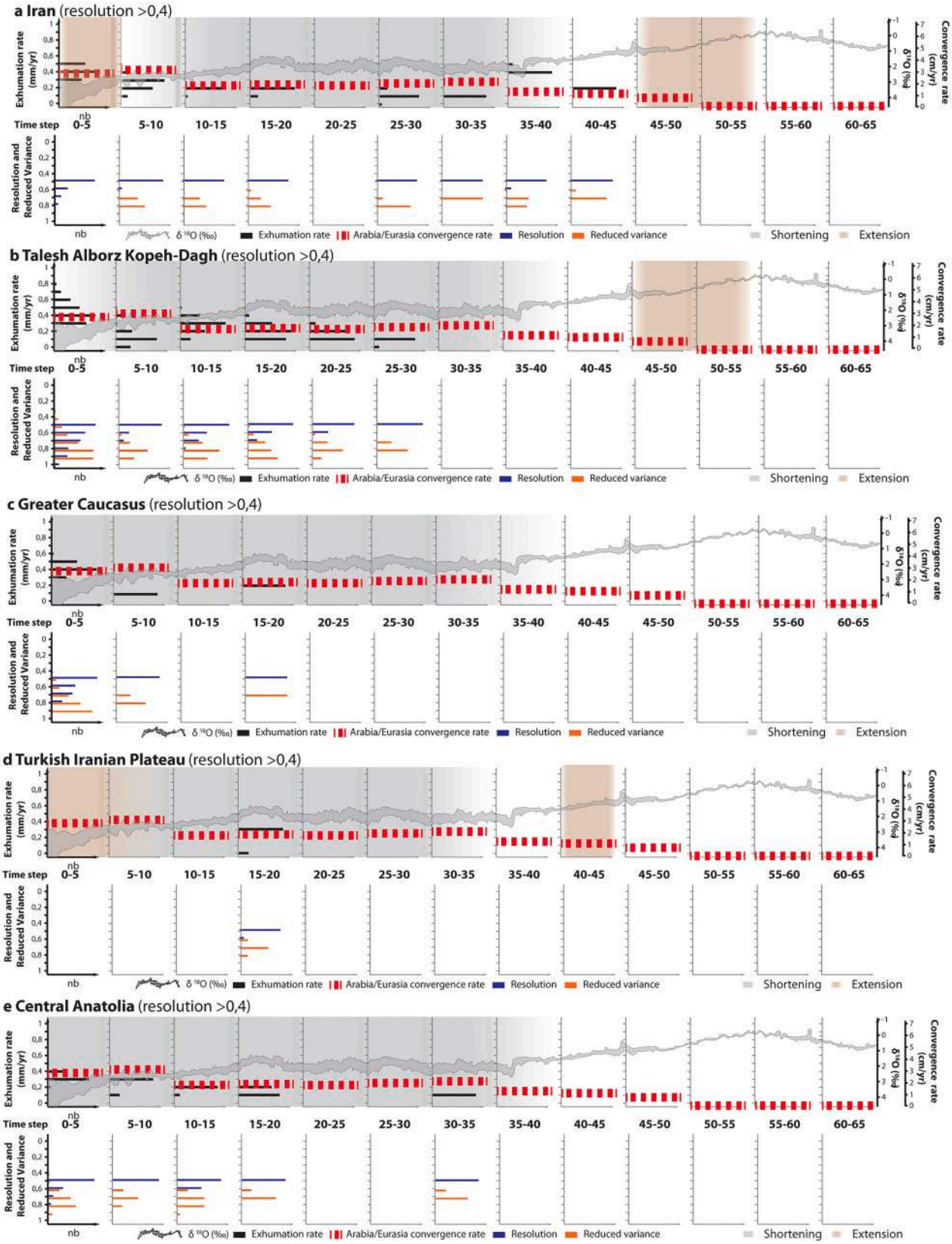

Fig. 6. Inferred exhumation rates through time for specific regions with potential climate and tectonic drivers. For each region, upper figure shows plate convergence and subduction velocity as red dashed line, with shaded zones representing documented periods of extension and shortening (pink and grey, respectively). Global oxygen isotope climate proxy curve shown in continuous grey shading. Exhumation rates for region shown as black bar graph. Lower figure shows values of resolution and reduced resolution of the ages shown above. Results are shown only for rates with a temporal resolution above 0.4. (For interpretation of the references to color in this figure legend, the reader is referred to the web version of this article.)

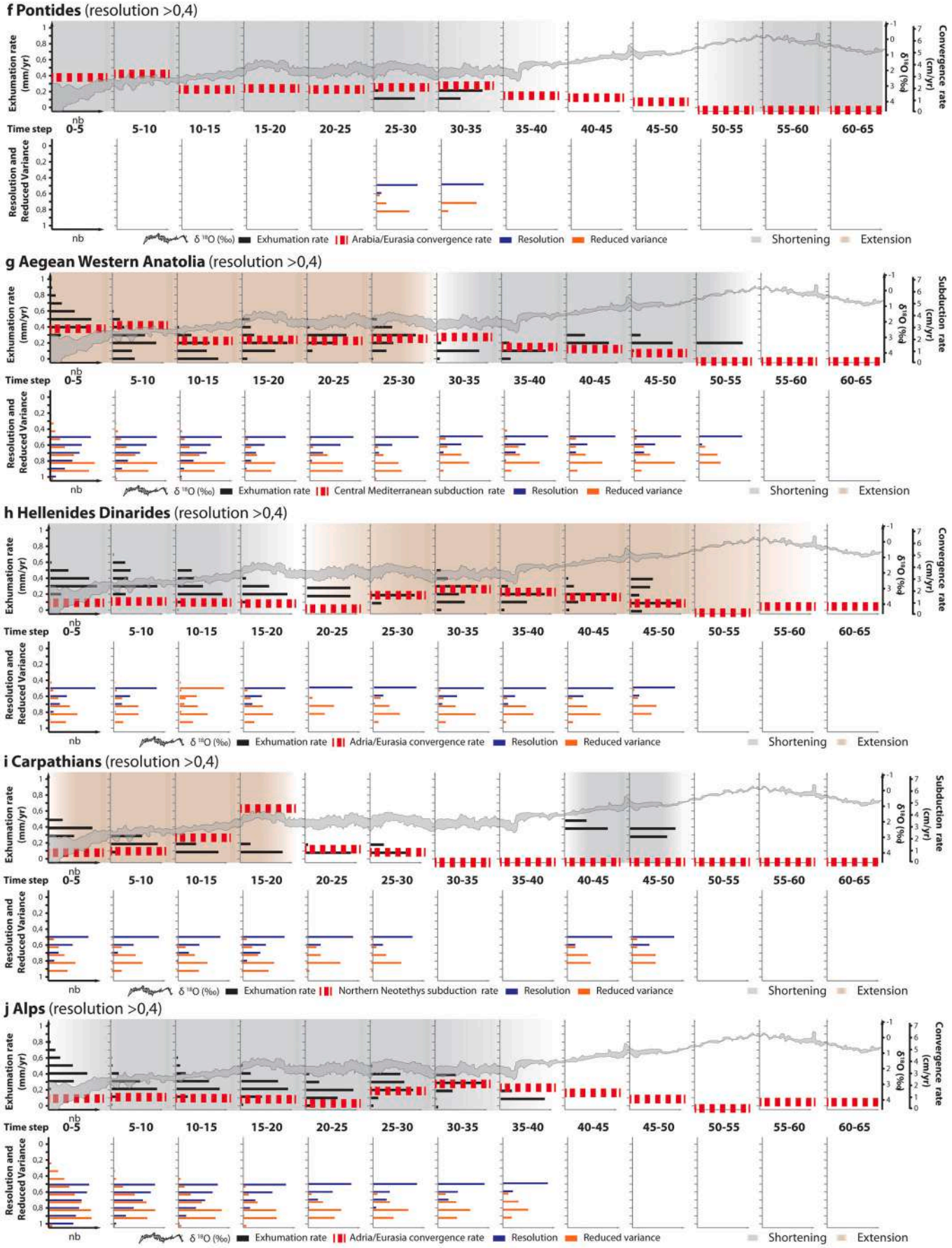

Fig. 6. (*continued*).

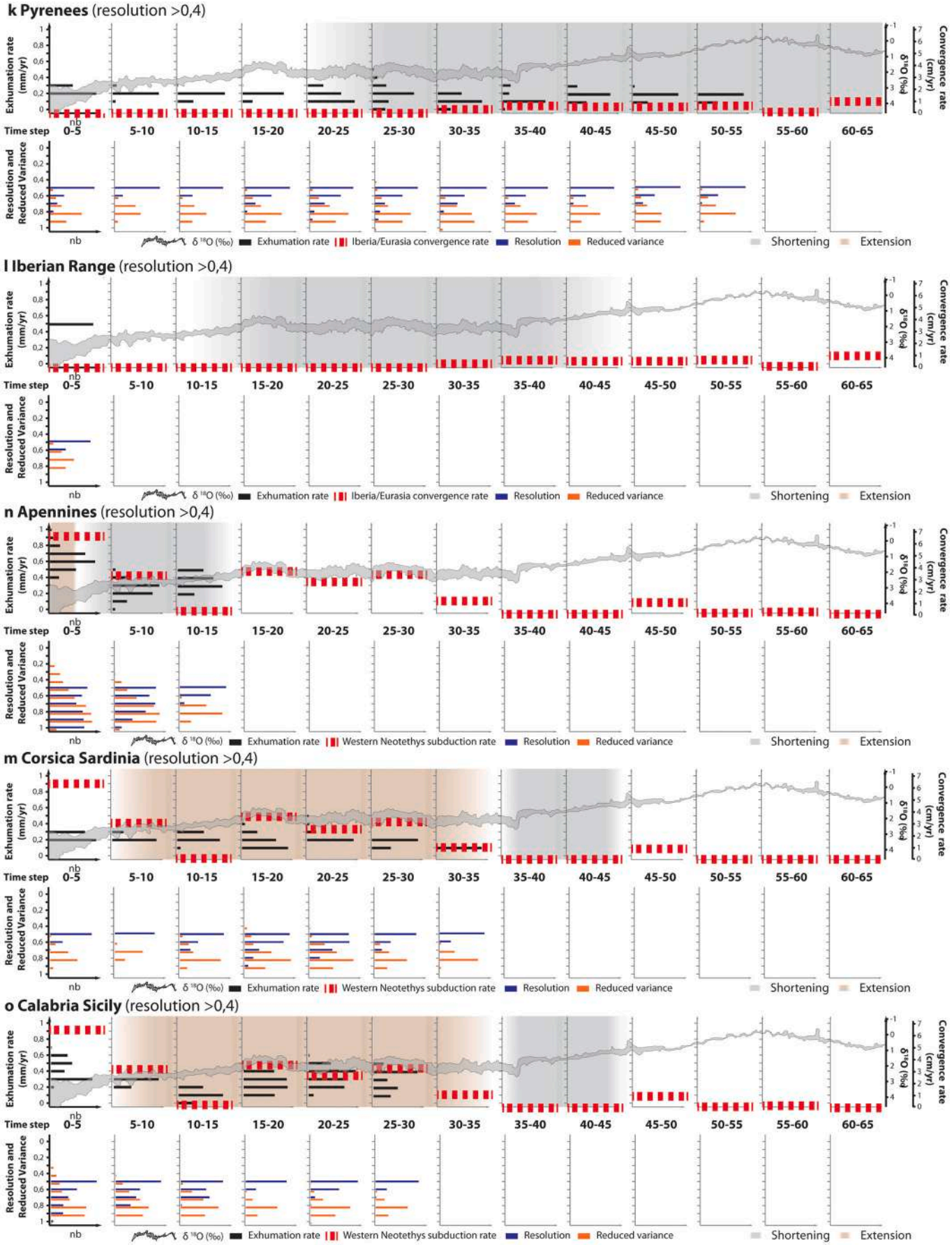

Fig. 6. (*continued*).

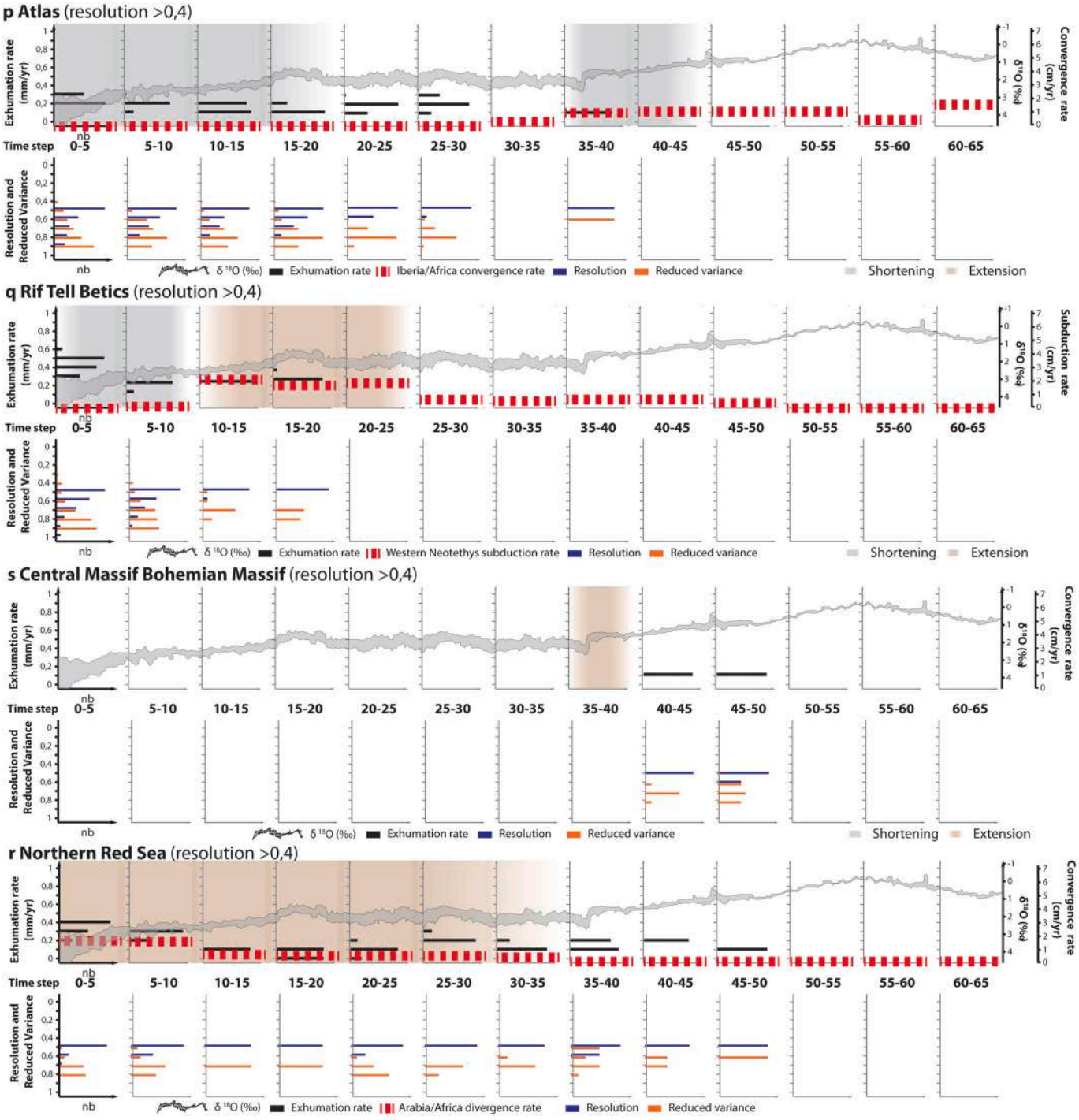

Fig. 6. (*continued*).

modal values increase to 0.5 and 0.4 mm/yr (from 0.4 and 0.3 mm/yr) in the Iran block, to 0.8 and 0.4 mm/yr (from 0.4 and 0.1 mm/yr) in the TAK block, to 0.6 and 0.4 mm/yr (both from 0.1 mm/yr) in the Greater Caucasus, to 0.4 mm/yr (from 0.3 mm/yr for the maximum rates) while modal rates remain constant (0.3 mm/yr) in Central Anatolia, to 1 and 0.5 mm/yr (from 0.6 and 0.2 mm/yr) in the Aegean Western Anatolia, to 0.8 and 0.4 mm/yr (from 0.5 and 0.2 mm/yr) in the Alps, to 0.5 and 0.4 mm/yr (from 0.3 and 0.2 mm/yr) in the Carpathians, to 1 and 0.6 mm/yr (from 0.5 and 0.3 mm/yr) in the Apennines, to 0.6 from 0.3 mm/yr (maximum rates) while the mode remains constant (0.3 mm/yr) in Calabria Sicily block, to 0.6 and 0.5 mm/yr (both from 0.2 mm/yr) in the Rif Tell Betics, to 0.4 from 0.3 mm/yr (for both maximum and modal rates) in the Northern Red Sea and to 0.5 mm/yr from unresolved rates for both maximum and modal rates in the Iberia Block. The remaining blocks do not present thermochronologic ages to resolve exhumation rates over the last 5 and 10 Ma (Turkish Iranian Plateau, Pontides Central/Bohemian Massifs) or show little changes that may not be statistically significant (Hellenides-Dinarides, Pyrenees, Corsica Sardinia and Atlas tectonic blocks; (Figs. 5L, M, 6).

4. Tectonic interpretation

Although variations in exhumation rates within individual blocks may record local orogenic (e.g., outward orogenic growth or out of

sequence deformation; strain partitioning, etc.) or extensional processes (e.g., core complex development), the considerable number of cooling ages used to calculate the inferred rates provide a measure of the rates of exhumation activity within the regional block. Thus, we expect that our inferred rates characterize the cooling history of rocks belonging yo tectonically active parts of each block. In the following, we interpretate these exhumation rates in the context of our kinematic model and the tectonic events (i.e., oceanic subduction, continental collision, and back-arc extension) that characterized the Neo-Tethys subduction zone (i.e., Middle East, Adria, and Western Mediterranean).

4.1. Arabia-Eurasia collision

During the Late Cretaceous and throughout the early Paleogene, the northward motion of Africa and Arabia led to the progressive closure of the Tethyan ocean (Fig. 5A and B; e.g. Agard et al., 2011; Seton et al., 2012b; van Hinsbergen et al., 2020). The onset of the Arabia-Eurasia collision is controversial (e.g. Berberian and King, 1981), although an increasing number of study has placed it around the late Eocene–-Oligocene (35–26 Ma, e.g. Ballato et al., 2011; Mouthereau et al., 2012; McQuarrie and van Hinsbergen, 2013; Barber et al., 2018; Koshnaw et al., 2018) possibly within an overall south-eastward younging trend (Darin and Umhoefer, 2022).

In our model, the onset of well-resolved exhumation rates (i.e., > 0.4) for the Iranian tectonic is in the 40–45 Ma time window (Figs. 5E and 6a) while an acceleration in exhumation rate occurs at 30–35 Ma (Figs. 5F and 6a). These data are consistent with the proposed onset of the Arabia-Eurasia collision during the late Eocene-early Oligocene. The TAK, the Greater Caucasus, and the Turkish Iranian plateau blocks, however, do not show well-resolved exhumation rates during that time window (Fig. 6b, c, and d). This observation agrees with field-based studies describing localized, moderate exhumation during the earliest stages of collision, followed by the deposition of unconformable clastic sediments in tectonic basins (e.g. Ballato et al., 2011; Cowgill et al., 2016; Paknia et al., 2021; Tadayon et al., 2017, 2019). After a decrease in the Oligocene, exhumation rates increase again from the middle Miocene in most of the Middle East blocks (Fig. 5J and K). This is in agreement with the increase in the shortening and exhumation rates recognized in the Zagros, Alborz, Turkish-Iranian block, and Caucasus most likely during the onset of the “hard” phase of the Arabia-Eurasia collision (i.e., following the subduction of the stretched passive Arabian margin; e.g. Ballato et al., 2018; Barber et al., 2018; Cavazza et al., 2018; Madanipour et al., 2017; Mouthereau, 2011; Rezaeian et al., 2012; Tadayon et al., 2019). These results indicate that the acceleration in exhumation rates occurred asynchronously across the different tectonic blocks of the Middle East.

In the Turkish-Iranian Plateau block, our inferred rates indicate up to 0.3 mm/yr of exhumation between 15 and 20 Ma while the resolution for younger and older time intervals is rather low. Although the exact timing of plateau uplift is unknown, the age of the last marine regression indicates that it must have occurred sometime after 17–16 Ma (e.g. Ballato et al., 2017). Several explanations have been proposed for explaining this vertical growth, such as slab break-off and tearing that led to an upward asthenospheric flow (e.g. Faccenna et al., 2006; Cosentino et al., 2012; Skolbeltsyn et al., 2014; Schildgen et al., 2012b), dynamic uplift associated with a mantle convection cell from the Afar plume to the Aegean or both (Faccenna et al., 2010), and collision related crustal thickening (Allen et al., 2013; Schildgen et al., 2012a; Topuz et al., 2017).

Starting from the late Miocene (10 Ma), we observe an increase in the inferred exhumation rates in most of the tectonic blocks of the Middle East (Fig. 6a, b and 6 c). Such a pattern may reflect an increase in plate convergence rates although it may have been enhanced by the Late Miocene global cooling (e.g., Zachos et al., 2008; see Supplementary Material 2) and possibly associated glacial erosion at least in high elevated areas such as the Caucasus and the Talesh-Alborz-Kopeh-Dagh blocks.

An exception to this trend is represented by the TAK, where our inferred exhumation rates decrease in the 10–5 Ma time window before the overall increase in Pliocene rates. This could reflect a shift in the locus of deformation across the collision zone from its northern edge toward its interior and in the Zagros. Alternatively, such a decrease could be related to the development of the orocline bending of the Talesh-Alborz-Kopeh Dagh range around the South Caspian Basin which was most likely accommodated by strike-slip faulting rather than crustal thickening and shortening processes (e.g. Cifelli et al., 2015; Madanipour et al., 2017; Mattei et al., 2017, 2019).

4.2. Adria-Eurasia collision

The Adria-Eurasia collision started during the late Cretaceous with the accretion of the eastern part of the Adria plate (i.e. the South Armenian block) to the southern Eurasian margin following the closure of the northern branch of the Neo-Tethys (Rolland et al., 2012; Schmid et al., 2008; van Hinsbergen et al., 2020). This collision led to shortening and exhumation in the NE sectors of the Adria terranes in association with widespread ophiolite obduction (e.g. Cavazza et al., 2019; Okay et al., 2018; Rolland et al., 2012; Srodoń et al., 2018)(Ballato et al., 2018; Srodoń et al., 2018).

Cenozoic exhumation in the Adria domain (Hellenides-Dinarides, Aegean-Western Anatolia and Carpathians blocks) starts in the Eocene (55 to 45 Ma; Figs. 5C, D, 6h and i) during the accretion of the central part of Adria to the Eurasian southern margin (e.g. Doglioni et al., 2002; Jolivet and Brun, 2010; Srodoń et al., 2018). The latest Eocene-earliest Oligocene, exhumation rates in the Aegean-Western Anatolia and the Hellenides-Dinarides blocks present a large dispersion (<0.1 to 0.6 mm/yr) in association with an acceleration in the subduction velocity (Fig. 6g and h). This acceleration is most likely related to the onset of trench rollback, which led to backarc extension in the inner Dinarides and the Rhodope during the early and middle Miocene, respectively (e.g. Burg, 2012; Ustaszewski et al., 2010), and in the Aegean Sea and in Crete during the middle-late Miocene (e.g. Jolivet et al., 2013; Figs. 5I to 5L). Similarly, the Carpathian slab started retreating in the Early Miocene (Carminati et al., 2013; Faccenna et al., 2014), although our modelled exhumation rates increase from 25 to 30 Ma (e.g., Gagała et al., 2012; Fig. 6i). Well-resolved exhumation rates for the Adrian domain occurs also in the Pontides block during the 25–35 Ma time windows (Figs. 5G, H and 6f) although the Pontides exhumation could reflect the earliest stages of the Arabia Eurasia collision (Ballato et al., 2018; Darin and Umhoefer, 2022).

In the Alps, the onset of continental collision with the subduction of the European margin beneath Adria started at 35–40 Ma (e.g. Burkhard and Sommaruga, 1998; Dielforder et al., 2016; Doglioni et al., 1997) (Fig. 6j). This event is associated with the first emergence of topography above sea level and is associated with the first erosion-related cooling ages (Schlunegger and Willett, 1999; Schmid et al., 2008) in agreement with well-resolved cooling ages during the 35–40 Ma time window (Fig. 6j). The pattern of exhumation rates through time for the Alps presents a high dispersion (<0.1 to 0.6 mm/yr) with modal rates of 0.2–0.3 mm/yr until 5 Ma (Fig. 6j) when exhumation rates increased. Throughout the Oligocene and the Miocene, collisional deformation led to the exhumation of the Eurasian crust in the hinterland of the orogen and the progressive incorporation of sedimentary cover and basement of the Eurasian margin and the overriding Adria plate into the wedge (e.g. Burkhard and Sommaruga, 1998; Carrapa et al., 2015; Dielforder et al., 2016; Zanchetta et al., 2015).

Overall, we link the exhumation patterns recorded in the Adria domain to the collision with Eurasia that started in the late Cretaceous and continued throughout the Cenozoic (Fig. 6g-m). Locally in the Carpathians, and in the Aegean-Western Anatolia tectonic blocks, the Neo-Tethys slab rollback and associated back-arc extension, controlled the exhumation patterns from the Oligocene until the present (Fig. 5). In

the eastern sectors of the Turkish-Iranian plateau and in central Anatolia exhumation could have been also controlled by deep-seated processes (see previous section). Our model, however, is not able to capture the late Miocene westward motion of the Anatolian microplate, probably because exhumation was limited and highly localized along the North Anatolian fault (e.g. Şengör et al., 2005).

As for the Middle East area, most of the blocks in the Adria domain, show an increase in exhumation rates from 5 Ma (e.g., Central Anatolia, Aegean-Western Anatolia, Carpathians and Alps, Fig. 6e, g, i, and j). Such an increase, however, is not recognized in Dinarides-Hellenides where rates are rather uniform (Fig. 6h), and in the Pontides (Fig. 6f) where rates are not resolved either because exhumation was too localized or because it has been limited resulting in thermochronological mostly older than 10 Ma (Fig. 6f and h).

4.3. *Iberia-Eurasia collision, Western Mediterranean slab roll-back, and Africa-Eurasia convergence*

In the Western Mediterranean domain, our modelled rates show a southward migration of the locus of exhumation throughout the Cenozoic with two major shifts (Fig. 5K). The oldest phase is recorded in the Pyrenees, with well resolved exhumation rates starting from 55 to 50 Ma (Fig. 5C). This result is consistent with the recent reassessment of cooling paths obtained from published low-temperature thermochronological data from Western Europe and North Africa (Mouthereau et al., 2021). The onset of erosional exhumation at 55–50 Ma was triggered by the counterclockwise rotation of the Iberian plate, which in turn led to the subduction of the highly extended Iberian continental margin and the Eocene continental collision (e.g. Vacherat et al., 2016 and reference therein). Interestingly, well resolved exhumation rates from 55 Ma were associated with topographic growth, which started 25 to 20 million years after the onset of the Pyrenean orogenesis (e.g., Curry et al., 2019). This lag time may have been caused by the deformation of the oceanic domain or the distal hyper-extended continental margin (Mouthereau et al., 2021 and references therein). The inferred exhumation rates present some accelerations until 25–20 Ma when a decrease in mean rates and variance occurs (Fig. 5K). To a first approximation, this pattern agrees with the results presented by Mouthereau et al. (2021).

The Oligocene marks the first regional-scale, southward shift in exhumation processes. Specifically, in the Corsica-Sardinia and the Sicily-Calabria blocks, the early and the late Oligocene, respectively, are characterized by the onset of extensional tectonics with denudation rates ranging from 0.1 to 0.5 mm/yr until the present (Figs. 5G to 5K, 6m and 6o). This is interpreted to reflect the Early Oligocene Western Alpine Tethys increase in the subduction rates that led to slab roll-back, and the subsequent opening, during the Miocene, of the Lion Gulf, the Algerian basin, and the Alboran Sea (e.g., Faccenna et al., 2014; Fellin et al., 2005). The opening of these back-arc basins may have been conditioned by the occurrence of rifting and volcanism in the Western European Rift System (Fig. 1; Mouthereau et al., 2021 and references therein).

Coeval with the roll-back of the Alpine Tethys slab, we observe a progressive decrease in exhumation rates in the Pyrenees block throughout the late Oligocene and the early-middle Miocene, most likely in response to the progressive ending of collisional deformation (Figs. 5H, I and 6k). The middle to late Miocene marks the second regional scale, southward migration of the locus of exhumation in the Western Mediterranean area. Our data document an increase in the inferred exhumation rates in both Atlas and Rif-Tell-Betics blocks from 30 and 20 Ma, respectively (Figs. 5H, J, 6p and q), according with previous published inversion models (e.g. Lanari et al., 2020a, 2020b; Mouthereau et al., 2021 and references therein). Exhumation in the Atlas is related to an increase in rock uplift rates due transpressional deformation along the north-western African margin (e.g., Lanari et al., 2020b; Soumaya et al., 2018; Gomez et al., 2000). This transpressional tectonic regime has been favored by the oblique, WNW-ESE oriented, convergence of Africa with respect to Eurasia since ~15 Ma (Dewey et al., 1989; DeMets et al., 1994; Serpelloni et al., 2007; Lanari et al., 2020b). This tectonics (and associated volcanism) is a straight consequence of slab break-off and the following westward drifting of the Gibraltar Arc that affected both north Africa and Iberia (e.g. Casalini et al., 2022; Duggen et al., 2009; Faccenna et al., 2004, 2014; Frizon de Lamotte et al., 2000; Mouthereau et al., 2021). Part of the increase in exhumation rates observed in the Rif Tell Betics and in the Atlas may be related to a regional surface uplift event induced by mantle upwelling associated with the complex Gibraltar arc evolution described earlier (e.g., Civiero et al., 2020) and/or with the Canary mantle plume (Duggen et al., 2009). Although in Iberia we do not have high-resolution exhumation rates prior to 5 Ma, large scale uplift and exhumation occurred in the Ebro Basin from ~10 to ~5 Ma, most likely in response to deep-seated processes (Rat et al., 2022). In any case, uplift in the Ebbro Basin was complete when the Messinian salinity crisis occurred (Rat et al., 2022) It is also unclear if such a deep processes are still producing large scale uplift in North Africa because along the major valleys of the Anti-Atlas alluvial aggradation has occurred through the Quaternary (e.g. Arboleya et al., 2008; Lanari et al., 2022).

Overall, we interpret the southward shift in the locus of exhumation as a consequence of different accommodation of the Africa-Eurasia plate convergence. Finally, it should be noted that we do not observe several localized accelerations, due to the limited resolution of our model, for example, the recent increase in exhumation rates in the Corsica-Sardinia tectonic block (Fellin et al., 2005), or recent rapid uplift in the Pontides of N Turkey (Ballato et al., 2018).

5. Discussion

5.1. *Tectonic control on exhumation rates*

The spatio-temporal patterns of our modelled exhumation rates and their comparison with the main tectonic settings (i.e., compression or extension) and associated velocities (i.e., plate convergence or subduction rates) enables recognizing the two major mechanisms driving exhumation and the lag time between the causes of exhumation and the response time of the thermochronometric systems.

One mechanism is related to tectonic denudation during extension in back-arc regions (Fig. 2). There, the increase in subduction velocity induced by trench retreat (e.g., Faccenna et al., 2004) predates by a few million years the increase in exhumation rates as observed in the Aegean-Western Anatolia, the Calabria-Sicily, and the Rif-Tell-Betics tectonic blocks (Fig. 6g, o and q). One exception to this pattern is from the Corsica Sardinia block (Fig. 6m), where subduction rates increased at 35 Ma in association with the onset of exhumation. In the Apennines, we do not observe a clear link between the acceleration in subduction velocity and exhumation rates (Fig. 6n), but this is probably due to lack of ages older than 15 Ma because most of the Apennines were below the sea level until the late Miocene or Pliocene (e.g. Erlanger et al., 2022; Fellin et al., 2021; San Jose et al., 2020).

The other mechanism is related to erosional exhumation during topographic growth induced by compressional deformation and continental collision (Fig. 2). In this case the overall exhumation pattern across different orogens is slightly different. In the Alps, the onset of collision during the late Eocene to early Oligocene (35–40 Ma, e.g., Burkhard and Sommaruga, 1998; Doglioni and Bosellini, 1987) corresponds to the first well-resolved increase in exhumation rates (Fig. 6j). This also happens in the Dinarides-Hellenides (e.g., van Hinsbergen et al., 2020 and references therein; Fig. 6h). In the Middle East, the onset of well-resolved exhumation rates at 40–45 Ma in the Iran block, is followed by a clear increase in exhumation rate and their dispersion at 35–40 Ma (Fig. 6a). Although the timing of the Arabia-Eurasia collision is still matter of debate, the 35–40 Ma increase in rates may reflect the earliest stages of collision (e.g., Berberian, 1981; Ballato et al., 2018; Darin and Umhoefer, 2022). In the Pyrenees, the oldest evidence of

collision is Eocene (e.g. Vacherat et al., 2016) while its waning stage is thought to initiate by early Miocene (~20 Ma; e.g. Chevrot et al., 2018; Muñoz, 1992; Olivet, 1996; Teixell et al., 2018). This pattern corresponds to well-resolved, highly dispersed exhumation rates from 55 to 20 Ma, followed by a decrease in the rate dispersion until the present (Fig. 6k).

Importantly, the end of collisional deformation is associated with the cessation of both outward propagation of the deformation fronts and rock uplift. Under these circumstances erosion is mostly controlled by the topographic relief of the decaying landscape (e.g., Braun and Robert, 2005), bedrock erodibility (e.g., Scharf et al., 2013), and the efficiency of surface processes which is primarily function of the precipitation regime (e.g., Bookhagen and Strecker, 2012). Through time, erosion rates are expected to decrease and become more uniform. This pattern seems to occur also in the Pyrenees (Fig. 6k), at least until 10 Ma, when our inferred exhumation rates show a slight increase that has been also documented by recent studies (Fillon et al., 2021; Huyghe et al., 2020; Rat et al., 2022). As a general outcome, these observations show that while collisional deformation is accompanied by an increase in both, the inferred exhumation rates and their dispersion, its termination is characterized by a decrease in erosion rates and in their dispersion.

5.2. Late Cenozoic climate change impact

There are several potential changes in climate that could have affected erosion rates over the Cenozoic. To explore the potential impact of climate changes we compare our erosion rates with the evolution of the deep-sea temperature inferred from the $\delta^{18}O$ on benthic foraminifera (Zachos et al., 2001; Fig. 6).

The Cenozoic is noted for an overall cooling of least 16 °C following the early Eocene climatic optimum (from ca. 50 Ma; e,g, Westerhold et al., 2020; Zachos et al., 2008). This process led to the development of continental ice sheets in Antarctica and in the northern hemisphere from 35 Ma with an intensification in the 3–2 Ma (particularly in Greenland), respectively. The establishment of glacial-interglacial cycles during the last 3–2 Ma is also associated with large oscillations in climate with periods of 20 to 100 kys. Combined, these two mechanisms are thought to promote an increase in exhumation rate through glacial erosion at high latitude/elevation and widespread fluvial incision during the transition between oscillating climatic regimes, particularly over the Quaternary, which we discuss below (e.g. Herman et al., 2013; Molnar, 2004; Molnar and England, 1990; Zhang et al., 2001).

There are also more regional effects associated with the closure of ocean circulation gateways in the Tethys. The late Eocene to early Oligocene Arabia-Eurasia collision (Fig. 5F and G) marks the beginning of the eastern Mediterranean gateway closure. The final closure occurred only during the middle to late Miocene (Fig. 5K, Tortonian, e.g. Popov et al., 2004). This caused a reorganization of oceanic circulation, which is thought to have induced the onset of desertification in North Africa (e.g. Hamon et al., 2013). Our data, however, do not exhibit any distinct, widespread change in exhumation rates in the eastern Mediterranean, suggesting that the closure did not induce a significant change in regional erosion rates. Similarly, the progressive shrinkage of the Para-Tethys which led to the final isolation of the Caspian from the Black Sea during the last 5 Ma (Forte and Cowgill, 2013) has not resulted in a resolvable change in rate.

During the late Miocene, after the accretion of the Rif onto the northern Africa plate and the end of extension in the Alboran Sea, the westernmost portion of the Mediterranean was affected by a new stage of compression induced by the northward motion of Africa (Fig. 5L). This promoted the closure of existing connections to the Atlantic and the isolation of the Mediterranean area from the Atlantic Ocean, inducing the Messinian salinity crisis, which was associated with a sea level drop of >1500 m (e.g. Cosentino et al., 2013; Jolivet et al., 2006). Some authors argued for an increase in the erosional flux either in response to the base level fall (Foeken et al., 2003), or to a wetter climate in the early Pliocene at the end of the salinity crisis (Willett et al., 2006). Considering the short duration (< 1 Ma; Cosentino et al., 2013) of the Messinian salinity crisis it is not possible to resolve this effect in our models with 5 Ma timesteps, although it is possible that the effect is reflected in the 0–5 Ma timestep.

Connected to the closure of the western Mediterranean gateway, there is a similar drop in the base level for drainages to the Caspian Sea. Here, the base level fall was longer-lived, lasting 2 to 3 Ma and was associated with the isolation of the Caspian Sea, which received a large volume of sediments from the growing Caucasus and the already established Alborz (Ballato et al., 2015). The increase in inferred rates observed in the TAK in the last 5 Ma may be, at least in part, due to the base level drop of the Caspian Sea.

The largest potential change in exhumation rate associated with climate would have occurred in the latest Cenozoic as global cooling led to northern hemisphere glaciation and climate cyclicity (2 to 3 million years ago; Herman et al., 2013 and references therein). In fact, we observe an increase in exhumation rate for the last timestep of the inverse model for many regions. The largest changes are observed in the tectonic blocks of Iran, Talesh-Alborz-Kopeh-Dagh, Greater Caucasus, Aegean-Western Anatolia, Alps, Carpathians, Apennines, Calabria Sicily, and the Rif Tell Betics (Figs. 5, 6). In other regions, rates either do not increase (Turkish Iranian Plateau, Pontides, Hellenides-Dinarides, Pyrenees and Central-Bohemian Massifs) or exhibit only a small increase that may not be statistically significant (Central Anatolia, Corsica Sardinia, Northern Red Sea and Atlas; Figs. 5, 6). Given the parametrization with 5 Ma timesteps, however, we cannot differentiate an increase in rate over the last 2 Ma from the last 5 Ma.

As is always the case, we cannot differentiate a tectonic cause from a climate-induced cause for observed increases in exhumation rate (Willett et al., 2021). However, we can note other evidence for changes in tectonic forcing. For example, we can see that in some regions, the inferred rates started to increase earlier than 5 Ma (15 Ma Calabria-Sicily, 10 Ma Iran, Greater Caucasus, Aegean-Western Anatolia, Central Anatolia, Carpathians and Northern Red Sea), suggesting that tectonic-driven exhumation was increasing prior to any potential climate change. In contrast, in other cases, tectonic evidence suggests a decrease in convergence rate (Alps, Carpathians), even as exhumation rates increased.

Any effects of climate-enhanced erosion should be most pronounced in tectonically active areas. High relief, high elevation topography is more susceptible to enhanced surface erosion, and enhanced erosion rates can trigger a positive feedback whereby tectonic uplift further accelerates due to reduced gravitational loading as rock is removed by erosion (Whipple, 2009; Willett et al., 2001). This is also true for regions without active tectonics, but which still retain high relief from recently active tectonics. Such topography will also induce positive feedback in response to enhanced erosion through isostatic rebound in response to erosional unloading. Uplift feedback could play a role in the exhumation of the Alps, the Carpathians, and the Greater Caucasus, and possibly some of the areas with only small increases in erosion rate (Pyrenees, Corsica Sardinia, and Atlas). The areas that did not experience any increase in exhumation rates over the last 5 Ma are either tectonically inactive and/or dominated by low topographic relief (Central-Bohemian Massifs and Turkish Iranian Plateau). Another block that is actively deforming but does not present any increase in modelled exhumation rates is the Pontides. There, however, the generation of topographic relief through shortening and thickening processes started sometime after 10 Ma most likely in response to the westward motion of Anatolia along the North Anatolian Fault but this has not been fully reflected in the thermochronology data (e.g., Ballato et al., 2018).

In conclusion, the observation of higher rates in regions without other evidence of enhanced tectonic activity over the last 5 Ma, combined with the widespread occurrence of the rate increase suggests that such an increase could be linked to the late Cenozoic cooling and the increase in climate cyclicity.

6. Conclusions

In this study we investigate the effect of the demise of the Neo-Tethys, and the progressive collision of Arabia and Adria with Eurasia as reflected in the thermochronometric ages and exhumation patterns in the orogenic belts across the region. By compiling and designing an inverse model analysis of >7300 thermochronometric ages with our tectonic reconstruction, we obtain a comprehensive picture of the kinematics and associated erosion rates of the orogenic belts of the Mediterranean and Middle East region. Tectonic processes including subduction, collision, and extension induced by trench retreat result in topographic relief creation, erosion and exhumation. This is well documented by the positive correlation between exhumation and tectonic deformation rates. At a temporal resolution of 5 Ma and spatial scale of about 25 km, our data can resolve the timing of tectonic activity within individual orogenic belts rather than at the scale of single tectonic structures. Tectonic activity is also evident in the dispersion of inferred exhumation rates, with a larger variance in exhumation rate during active tectonics, and a lower variance during times of tectonic quiescence, including the immediate post-tectonic period.

Exhumation associated with tectonic uplift and erosion in response to changes in climate cannot be explicitly differentiated. Most changes in exhumation rates are associated with tectonic activity. However, we do observe an increase in exhumation rates over most of the Mediterranean and Middle East in the last 5 Ma. This increase is clearly highlighted in areas of active tectonics and/or high topographic relief associated with active or recent tectonic activity. Although we cannot rule out a tectonic contribution to some of these higher rates, the observation of higher rates in regions without other evidence of enhanced tectonic activity, as well as the widespread nature of the rate increase provides circumstantial evidence that this is in response to late Cenozoic cooling and the increase in climate cyclicity.

Declaration of Competing Interest

The authors declare that they have no known competing financial interests or personal relationships that could have appeared to influence the work reported in this paper.

Data availability

Data will be made available on request.

Acknowledgments

The authors would like to thank the Editor Timothy Kusky, two anonymous reviewers and Frédéric Mouthereau for detailed reviews and for pointing out some important studies that helped us to improve this study. R.L., A.B., C.F. and P.B., were supported by Prin2017-2020 (Geodynamics of the Arabia-Eurasia collisional zones, PI C. Faccenna, and MIUR (Ministry of Education University and Research), Excellence Department Initiative granted to the Department of Science, University of Roma Tre, (Art. 1, com. 314-337, Low 232/2016). P.B. was also supported by the MIUR (Rita Levi Montalchini grant).

Appendix A. Supplementary data

Supplementary data to this article can be found online at https://doi.org/10.1016/j.earscirev.2023.104328.

References

Agard, P., Omrani, J., Jolivet, L., Whitechurch, H., Vrielynck, B., Spakman, W., Monié, P., Meyer, B., Wortel, R., 2011. Zagros orogeny: a subduction-dominated process. Geol. Mag. 148, 692–725. https://doi.org/10.1017/S001675681100046X.

Allen, M.B., Saville, C., Blanc, E.J.P., Talebian, M., Nissen, E., 2013. Orogenic plateau growth: expansion of the Turkish-Iranian Plateau across the Zagros fold-and-thrust belt. Tectonics 32, 171–190. https://doi.org/10.1002/tect.20025.

Amante, C., Eakins, B.W., 2009. ETOPO1 1 Arc-Minute Global Relief Model: Procedures, Data Sources and Analysis. NOAA Tech. Memo. NESDIS NGDC-24. https://doi.org/10.1594/PANGAEA.769615.

Angrand, P., Mouthereau, F., 2021. Evolution of the Alpine orogenic belts in the Western Mediterranean region as resolved by the kinematics of the Europe-Africa diffuse plate boundary. Bsgf - Earth Sci. Bull. https://doi.org/10.1051/bsgf/2021031.

Arboleya, M.-L., Babault, J., Owen, L.A., Teixell, A., Finkel, R.C., 2008. Timing and nature of Quaternary fluvial incision in the Ouarzazate foreland basin, Morocco. J. Geol. Soc. London. 165, 1059–1073. https://doi.org/10.1144/0016-76492007-151.

Ballato, P., Cifelli, F., Heidarzadeh, G., Ghassemi, M.R., Wickert, A.D., Hassanzadeh, J., Dupont-Nivet, G., Balling, P., Sudo, M., Zeilinger, G., 2017. Tectono-sedimentary evolution of the northern Iranian Plateau: insights from middle–late Miocene foreland-basin deposits. Basin Res. 29, 417–446.

Ballato, P., Landgraf, A., Schildgen, T.F., Stockli, D.F., Fox, M., Ghassemi, M.R., Kirby, E., Strecker, M.R., 2015. The growth of a mountain belt forced by base-level fall: tectonics and surface processes during the evolution of the Alborz Mountains,N Iran. Earth Planet. Sci. Lett. 425, 204–218. https://doi.org/10.1016/j.epsl.2015.05.051.

Ballato, P., Parra, M., Schildgen, T.F., Dunkl, I., Yıldırım, C., Özsayın, E., Sobel, E.R., Echtler, H., Strecker, M.R., 2018. Multiple exhumation phases in the Central Pontides (N Turkey): new temporal constraints on major geodynamic changes associated with the closure of the neo-tethys ocean. Tectonics 37, 1831–1857. https://doi.org/10.1029/2017TC004808.

Ballato, P., Uba, C.E., Landgraf, A., Strecker, M.R., Sudo, M., Stockli, D.F., Friedrich, A., Tabatabaei, S.H., 2011. Arabia-Eurasia continental collision: insights from late Tertiary foreland-basin evolution in the Alborz Mountains, northern Iran. Bulletin 123, 106–131.

Barber, D.E., Stockli, D.F., Horton, B.K., Koshnaw, R.I., 2018. Cenozoic exhumation and foreland basin evolution of the Zagros Orogen during the Arabia-Eurasia Collision, Western Iran. Tectonics 37, 4396–4420. https://doi.org/10.1029/2018TC005328.

Barrier, É., Vrielynck, B., 2008. Palaeotectonic map of the Middle East, Atlas of 14 maps, tectonosedimentary-palinspastic maps from Late Norian to Pliocene. Comm. Geol. Map World (CCMW, CCGM), Paris, F.

Berberian, M., 1981. Zagros, Hindu Kush, Himalaya: Geodynamic Evolution, Geodynamics Series. https://doi.org/10.1029/GD003.

Berberian, M., King, G.C.P., 1981. Towards a paleogeography and tectonic evolution of Iran. Can. J. Earth Sci. 18, 210–265. https://doi.org/10.1139/e81-019.

Billi, A., Faccenna, C., Bellier, O., Minelli, L., Neri, G., Piromallo, C., Presti, D., Scrocca, D., Serpelloni, E., 2011. Recent tectonic reorganization of the Nubia-Eurasia convergent boundary heading for the closure of the western Mediterranean. Bull. la Société Géologique Fr. 182, 279–303.

Bookhagen, B., Strecker, M.R., 2012. Spatiotemporal trends in erosion rates across a pronounced rainfall gradient: examples from the southern Central Andes. Earth Planet. Sci. Lett. 327, 97–110.

Boutoux, A., Briaud, A., Faccenna, C., Ballato, P., Rossetti, F., Blanc, E., 2021. Slab folding and surface deformation of the Iran mobile belt. Tectonics v. 40 (6) e2020TC006300.

Braun, J., 2003. Pecube: a new finite-element code to solve the 3D heat transport equation including the effects of a time-varying, finite amplitude surface topography. Comput. Geosci. 29, 787–794.

Braun, J., 2002. Estimating exhumation rate and relief evolution by spectral analysis of age-elevation datasets. Terra Nov. 14, 210–214. https://doi.org/10.1046/j.1365-3121.2002.00409.x.

Braun, J., Robert, X., 2005. Constraints on the rate of post-orogenic erosional decay from low-temperature thermochronological data: application to the Dabie Shan, China. Earth Surf.Process. Landforms J. Br. Geomorphol. Res. Gr. 30, 1203–1225.

Burg, J.-P., 2012. Rhodope: from Mesozoic convergence to Cenozoic extension. Review of petro-structural data in the geochronological frame. J. Virtual Explor. 42, 1–44.

Burkhard, M., Sommaruga, A., 1998. Evolution of the western Swiss Molasse basin: structural relations with the Alps and the Jura belt. Geol. Soc. Spec. Publ. 134, 279–298. https://doi.org/10.1144/GSL.SP.1998.134.01.13.

Carminati, E., Doglioni, C., Gelabert, B., Panza, G., Raykova, R.B., Roca, E., Sabat, F., Scrocca, D., 2013. Evolution of the western Mediterranean.

Carminati, E., Lustrino, M., Doglioni, C., 2012. Geodynamic evolution of the central and western Mediterranean: Tectonics vs. Igneous petrology constraints. Tectonophysics 579, 173–192.

Carrapa, B., DeCelles, P.G., Wang, X., Clementz, M.T., Mancin, N., Stoica, M., Kraatz, B., Meng, J., Abdulov, S., Chen, F., 2015. Tectono-climatic implications of Eocene Paratethys regression in the Tajik basin of Central Asia. Earth Planet. Sci. Lett. 424, 168–178.

Casalini, M., Tommasini, S., Guarnieri, L., Avanzinelli, R., Lanari, R., Mattei, M., Conticelli, S., 2022. Subduction-related lamproitic signature in intraplate-like volcanic rocks: the case study of the Tallante alkali basalts, Betic Chain, South-Eastern Spain. Ital. J. Geosci. 141, 144–159.

Cavazza, W., Albino, I., Galoyan, G., Zattin, M., Cattò, S., 2019. Continental accretion and incremental deformation in the thermochronologic evolution of the Lesser Caucasus. Geosci. Front. 10, 2189–2202.

Cavazza, W., Cattò, S., Zattin, M., Okay, A.I., Reiners, P., 2018. Thermochronology of the Miocene Arabia-Eurasia collision zone of southeastern Turkey. Geosphere 14, 2277–2293.

Chevrot, S., Sylvander, M., Diaz, J., Martin, R., Mouthereau, F., Manatschal, G., Masini, E., Calassou, S., Grimaud, F., Pauchet, H., 2018. The non-cylindrical crustal architecture of the Pyrenees. Sci. Rep. 8, 1–8.

Cifelli, F., Ballato, P., Alimohammadian, H., Sabouri, J., Mattei, M., 2015. Tectonic magnetic lineation and oroclinal bending of the Alborz range: implications on the Southern Caspian Geodynamics. Tectonics 116–132. https://doi.org/10.1002/2014TC003626.Received.

Civiero, C., Custódio, S., Duarte, J.C., Mendes, V.B., Faccenna, C., 2020. Dynamics of the Gibraltar arc system: a complex interaction between plate convergence, slab pull, and mantle flow. J. Geophys. Res. Solid Earth 125 (7), e2019JB018873.

Cosentino, D., Buchwaldt, R., Sampalmieri, G., Iadanza, A., Cipollari, P., Schildgen, T.F., Hinnov, L.A., Ramezani, J., Bowring, S.A., 2013. Refining the Mediterranean "Messinian gap" with high-precision U-Pb zircon geochronology, central and northern Italy. Geology 41, 323–326.

Cosentino, D., Schildgen, T.F., Cipollari, P., Faranda, C., Gliozzi, E., Hudáčková, N., Lucifora, S., Strecker, M.R., 2012. Late Miocene surface uplift of the southern margin of the Central Anatolian plateau, Central Taurides,Turkey. Bull. Geol. Soc. Am. 124, 133–145. https://doi.org/10.1130/B30466.1.

Cowgill, E.S., Forte, A.M., Niemi, N.A., Avdeev, B., Tye, A., Trexler, C.C., Javakhishvili, Z., Elashvili, M., Godoladze, T., 2016. Relict basin closure and crustal shortening budgets during continental collision: an example from Caucasus sediment provenance. Tectonics 35, 2918–2947. https://doi.org/10.1002/2016TC004295.

Curry, M.E., van der Beek, P., Huismans, R.S., Wolf, S.G., Muñoz, J.-A., 2019. Evolving paleotopography and lithospheric flexure of the Pyrenean Orogen from3D flexuralmodeling and basin analysis. Earth Planet. Sci. Lett. 515, 26–37. https://doi.org/10.1016/j.epsl.2019.03.009.

Darin, M.H., Umhoefer, P.J., 2022. Diachronous initiation of Arabia-Eurasia collision from eastern Anatolia to the southeastern Zagros Mountains since middle Eocene time. Int. Geol. Rev. 1–29.

Davies, J.H., 2013. Global map of solid Earth surface heat flow. Geochem.Geophys. Geosyst. 14, 4608–4622. https://doi.org/10.1002/ggge.20271.

DeMets, C., Gordon, R.G., Argus, D.F., Stein, S., 1994. Effect of recent revisions to the geomagnetic reversal time scale on estimates of current plate motions. Geophys. Res. Lett. 21 (20), 2191–2194.

Dewey, J.F., Helman, M.L., Knott, S.D., Turco, E., Hutton, D.H.W., 1989. Kinematics of the western Mediterranean. Geochem. Soc. Spec. Publ. 45 (1), 265–283.

Dewey, J.F., Şengör, A.M.C., 1979. Aegean and surrounding regions: complex multiplate and continuum tectonics in a convergent zone. Geol. Soc. Am. Bull. 90, 84–92.

Dielforder, A., Berger, A., Herwegh, M., 2016. The accretion of foreland basin sediments during early stages of continental collision in the European Alps and similarities to accretionary wedge tectonics. Tectonics 35, 2216–2238.

Dodson, M.H., 1973. Closure temperature in cooling geochronological and petrological systems. Contrib. Min. Petrol. 40, 259–274.

Doglioni, C., Agostini, S., Crespi, M., Innocenti, F., Manetti, P., Riguzzi, F., Savascin, Y., 2002. On the extension in western Anatolia and the Aegean Sea. J. Virtual Explor. 8, 169–183.

Doglioni, C., Bosellini, A., 1987. Eoalpine and mesoalpine tectonics in the Southern Alps. Geol. Rundschau 76, 735–754.

Doglioni, C., Gueguen, E., Sàbat, F., Fernandez, M., 1997. The western Mediterranean extensional basins and the Alpine orogen. Terra Nov. 9, 109–112.

Duggen, S., Hoernle, K.A., Hauff, F., Klügel, A., Bouabdellah, M., Thirlwall, M.F., 2009. Flow of Canary mantle plume material through a subcontinental lithospheric corridor beneath Africa to the Mediterranean. Geology 37, 283–286. https://doi.org/10.1130/G25426A.1.

Ehlers, T.A., Farley, K.A., 2003. Apatite (U–Th)/He thermochronometry: methods and applications to problems in tectonic and surface processes. Earth Planet. Sci. Lett. 206, 1–14.

Erlanger, E.D., Fellin, M.G., Willett, S.D., 2022. Exhumation and erosion of the Northern Apennines, Italy: new insights from low-temperature thermochronometers. Solid Earth 13, 347–365.

Faccenna, C., Becker, T.W., 2020. Topographic expressions of mantle dynamics in the Mediterranean. Earth-Sci. Rev. 103327.

Faccenna, C., Becker, T.W., Auer, L., Billi, A., Boshi, L., Brun, J.P., Capitanio, F.A., Funiciello, F., Horvàth, F., Jolivet, L., Piromallo, C., 2014. Reviews of Geophysics Mantle dynamics in the Mediterranean. Rev. Geophys. 52, 283–332. https://doi.org/10.1002/2013RG000444.

Faccenna, C., Becker, T.W., Lallemand, S., Lagabrielle, Y., Funiciello, F., Piromallo, C., 2010. Subduction-triggered magmatic pulses: a new class of plumes? Earth PlanetSci. Lett. 299, 54–68.

Faccenna, C., Bellier, O., Martinod, J., Piromallo, C., Regard, V., 2006. Slab detachment beneath eastern Anatolia: A possible cause for the formation of the North Anatolian fault. Earth Planet. Sci. Lett. 242 (1–2), 85–97.

Faccenna, C., Piromallo, C., Crespo-Blanc, A., Jolivet, L., Rossetti, F., 2004. Lateral slab deformation and the origin of the western Mediterranean arcs. Tectonics 23. https://doi.org/10.1029/2002TC001488.

Fellin, M.G., Picotti, V., Zattin, M., 2005. Neogene to Quaternary rifting and inversion in Corsica: retreat and collision in the western Mediterranean. Tectonics 24, 1–29. https://doi.org/10.1029/2003TC001613.

Fellin, M.G., San Jose, M., Faccenna, C., Willett, S.D., Cosentino, D., Lanari, R., Gourbet, L., Maden, C., 2021. Transition from slab roll-back to slab break-off in the central Apennines, Italy: Constraints from the stratigraphic and thermochronologic record. GSA Bull. 134 (7-8), 1916–1930. https://doi.org/10.1130/B36123.1.

Fillon, C., Mouthereau, F., Calassou, S., Pik, R., Bellahsen, N., Gautheron, C., Stockli, D., Brichau, S., Daril, N., Mouchené, M., van der Beek, P., 2021. Post-orogenic exhumation in the western Pyrenees: evidence for extension driven by pre-orogenic inheritance. J. Geol. Soc. Lond. 178, jgs2020-079 https://doi.org/10.1144/jgs2020-079.

Fitzgerald, P.G., Muñoz, J.A., Coney, P.J., Baldwin, S.L., 1999. Asymmetric exhumation across the Pyrenean orogen: implications for the tectonic evolution of a collisional orogen. Earth Planet. Sci. Lett. 173, 157–170.

Foeken, J.P.T., Dunai, T.J., Bertotti, G., Andriessen, P.A.M., 2003. Late Miocene to present exhumation in the Ligurian Alps (southwest Alps) with evidence for accelerated denudation during the Messinian salinity crisis. Geology 31, 797–800. https://doi.org/10.1130/G19572.1.

Forte, A.M., Cowgill, E., 2013. Late Cenozoic base-level variations of the Caspian Sea: a review of its history and proposed driving mechanisms. Palaeogeogr. Palaeoclimatol. Palaeoecol. 386, 392–407.

Fox, M., Herman, F., Willett, S.D., May, D.A., 2014. A linear inversion method to infer exhumation rates in space and time from thermochronometric data. Earth Surf. Dyn. 2, 47–65. https://doi.org/10.5194/esurf-2-47-2014.

Fox, M., Herman, F., Willett, S.D., Schmid, S.M., 2016. The exhumation history of the European Alps inferred from linear inversion of thermochronometric data. Am. J. Sci. 316 (6), 505–541.

Frizon de Lamotte, D., Leturmy, P., Missenard, Y., Khomsi, S., Ruiz, G., Saddiqi, O., Guillocheau, F., Michard, A., 2009. Mesozoic and Cenozoic vertical movements in the Atlas system (Algeria, Morocco, Tunisia): an overview. Tectonophysics 475, 9–28. https://doi.org/10.1016/j.tecto.2008.10.024.

Frizon de Lamotte, D., Saint Bezar, B., Bracène, R., Mercier, E., 2000. The two main steps of the Atlas building and geodynamics of the western Mediterranean. Tectonics 19, 740–761.

Gagała, Ł., Vergés, J., Saura, E., Malata, T., Ringenbach, J., Werner, P., Krzywiec, P., 2012. Architecture and orogenic evolution of the northeastern Outer Carpathians from cross-section balancing and forward modeling. Tectonophysics 532–535, 223–241. https://doi.org/10.1016/j.tecto.2012.02.014.

Gallagher, K., Stephenson, J., Brown, R., Holmes, C., Fitzgerald, P., 2005. Low temperature thermochronology and modeling strategies for multiple samples 1: Vertical profiles. Earth Planet. Sci. Lett. 237, 193–208.

Gomez, F., Beauchamp, W., Barazangi, M., 2000. Role of the Atlas Mountains (northwest Africa) within the African-Eurasian plateboundary zone. Geology 28 (9), 775–778.

Gueguen, E., Doglioni, C., Fernandez, M., 1998. On the post-25 Ma geodynamic evolution of the western Mediterranean. Tectonophysics 298, 259–269.

Gvirtzman, Z., Faccenna, C., Becker, T.W., 2016. Tectonophysics Isostasy, flexure and dynamic topography. Tectonophysics 683, 255–271.

Hamon, N., Sepulchre, P., Lefebvre, V., Ramstein, G., 2013. The role of eastern tethys seaway closure in the middle miocene climatic transition (ca. 14 Ma). Clim. Past 9, 2687–2702. https://doi.org/10.5194/cp-9-2687-2013.

Handy, M.R., Schmid, S., Bousquet, R., Kissling, E., Bernoulli, D., 2010. Reconciling plate-tectonic reconstructions of Alpine Tethys with the geological-geophysical record of spreading and subduction in the Alps. Earth-Sci. Rev. 102, 121–158. https://doi.org/10.1016/j.earscirev.2010.06.002.

Herman, F., Seward, D., Valla, P.G., Carter, A., Kohn, B., Willett, S.D., Ehlers, T.A., 2013. Worldwide acceleration of mountain erosion under a cooling climate. Nature 504, 423–426. https://doi.org/10.1038/nature12877.

Huyghe, D., Mouthereau, F., Ségalen, L., Furió, M., 2020. Long-term dynamic topographic support during post-orogenic crustal thinning revealed by stable isotope (δ18O) paleo-altimetry in eastern Pyrenees. Sci. Rep.-UK 10, 2267. https://doi.org/10.1038/s41598-020-58903-w.

Jiao, R., Herman, F., Seward, D., 2017. Late Cenozoic exhumation model of New Zealand: Impacts from tectonics and climate. Earth-Sci. Rev. 166, 286–298.

Jolivet, L., Augier, R., Robin, C., Suc, J.P., Rouchy, J.M., 2006. Lithospheric-scale geodynamic context of the Messinian salinity crisis. Sediment. Geol. 188–189, 9–33. https://doi.org/10.1016/j.sedgeo.2006.02.004.

Jolivet, L., Brun, J.-P., 2010. Cenozoic geodynamic evolution of the Aegean. Int. J. Earth Sci. 99, 109–138.

Jolivet, L., Faccenna, C., 2000. Mediterranean extension and the Africa-Eurasia collision. Tectonics 19, 1095–1106.

Jolivet, L., Faccenna, C., Huet, B., Labrousse, L., Le Pourhiet, L., Lacombe, O., Lecomte, E., Burov, E., Denèle, Y., Brun, J.-P., et al., 2013. Aegean tectonics: strain localisation, slab tearing and trench retreat. Tectonophysics 597–598, 1–33.

Koshnaw, R.I., Stockli, D.F., Schlunegger, F., 2018. Timing of the Arabia-Eurasia continental collision-evidence from detrital zircon U-Pb geochronology of the Red Bed Series strata of the northwest Zagros hinterland, Kurdistan region of Iraq. Geology 47, 47–50. https://doi.org/10.1130/G46438Y.1.

Lanari, R., Faccenna, C., Fellin, M.G., Essaifi, A., Nahid, A., Medina, F., Youbi, N., 2020a. Tectonic evolution of the western high Atlas of Morocco: oblique convergence reactivation and transpression. Tectonics 39 (3), e2019TC005563.

Lanari, R., Fellin, M.G., Faccenna, C., Balestrieri, M.L., Pazzaglia, F.J., Youbi, N., Maden, C., 2020b. Exhumation and surface evolution of the western high atlas and surrounding regions as constrained by low-temperature thermochronology. Tectonics 39 (3), e2019TC005562.

Lanari, R., Reitano, R., Giachetta, E., Pazzaglia, F.J., Clementucci, R., Faccenna, C., Fellin, M.G., 2022. Is the Anti-Atlas of Morocco still uplifting? J. AfricanEarth Sci. 104481.

Madanipour, S., Ehlers, T.A., Yassaghi, A., Enkelmann, E., 2017. Accelerated middle Miocene exhumation of the Talesh Mountains constrained by U-Th/He thermochronometry: evidence for the Arabia-Eurasia collision in the NW Iranian Plateau. Tectonics 36, 1538–1561.

Malinverno, A., Ryan, W.B.F., 1986. Extension in the Tyrrhenian Sea and shortening in the Apennines as result of arc migration driven by sinking of the lithosphere. Tectonics 5, 227–245.

Malusà, M.G., Faccenna, C., Garzanti, E., Polino, R., 2011. Divergence in subduction zones and exhumation of high pressure rocks (Eocene Western Alps). Earth Planet. Sci. Lett. 310, 21–32.

Mattei, M., Cifelli, F., Alimohammadian, H., Rashid, H., Winkler, A., Sagnotti, L., 2017. Oroclinal bending in the Alborz Mountains (Northern Iran): new constraints on the age of South Caspian subduction and extrusion tectonics. Gondwana Res. 42, 13–28. https://doi.org/10.1016/j.gr.2016.10.003.

Mattei, M., Visconti, A.L., Cifelli, F., Nozaem, R., Winkler, A., Sagnotti, L., 2019. Clockwise paleomagnetic rotations in northeastern Iran: Major implications on recent geodynamic evolution of outer sectors of the Arabia-Eurasia collision zone. Gondwana Res. 71, 194–209.

McQuarrie, N., van Hinsbergen, D.J.J., 2013. Retrodeforming the Arabia-Eurasia collision zone: age of collision versus magnitude of continental subduction. Geology 41, 315–318.

Menant, A., Jolivet, L., Vrielynck, B., 2016. Kinematic reconstructions and magmatic evolution illuminating crustal and mantle dynamics of the eastern Mediterranean region since the late Cretaceous. Tectonophysics 675, 103–140. https://doi.org/10.1016/j.tecto.2016.03.007.

Molnar, P., 2004. Late Cenozoic increase in accumulation rates of terrestrial sediment: how might climate change have affected erosion rates? Annu. Rev. Earth Planet. Sci. 32, 67–89.

Molnar, P., England, P., 1990. Late Cenozoic uplift of mountain ranges and global climate change: chicken or egg? Nature 346, 29–34.

Mouthereau, F., 2011. Timing of uplift in the Zagros belt/Iranian plateau and accommodation of late Cenozoic Arabia-Eurasia convergence. Geol. Mag. 148, 726–738. https://doi.org/10.1017/S0016756811000306.

Mouthereau, F., Angrand, P., Jourdon, A., Ternois, S., Fillon, C., Calassou, S., Chevrot, S., Ford, M., Jolivet, L., Manatschal, G., Masini, E., Thinon, I., Vidal, O., Baudin, T., 2021. Cenozoic mountain building and topographic evolution in Western Europe: impact of billions of years of lithosphere evolution and plate kinematics. Bsgf - Earth Sci Bulletin 192, 56. https://doi.org/10.1051/bsgf/2021040.

Mouthereau, F., Lacombe, O., Vergés, J., 2012. Building the Zagros collisional orogen: timing, strain distribution and the dynamics of Arabia/Eurasia plate convergence. Tectonophysics 532, 27–60.

Müller, R.D., Sdrolias, M., Gaina, C., Roest, W.R., 2008. Age, spreading rates, and spreading asymmetry of the world's ocean crust. Geochem. Geophys. Geosyst. 9.

Muñoz, J.A., 1992. Evolution of a continental collision belt: ECORS-Pyrenees crustal balanced cross-section. In: Thrust Tectonics. Springer, pp. 235–246.

Okay, A.I., 2008. Geology of Turkey: a synopsis. Anschnitt 21, 19–42.

Okay, A.I., Altiner, D., Sunal, G., Aygül, M., Akdoğan, R., Altiner, S., Simmons, M., 2018. Geological evolution of the Central Pontides. Geol. Soc. LondonSpec. Publ. 464, 33–67.

Olivet, J.L., 1996. Kinematics of the Iberian plate. Bull. des Centres RechExplor. Elf Aquitaine 20, 131–195.

Paknia, M., Ballato, P., Heidarzadeh, G., Cifelli, F., Hassanzadeh, J., Vezzoli, G., Mirzaie Ataabadi, M., Ghassemi, M.R., Mattei, M., 2021. Neogene tectono-stratigraphic evolution of the intermontane Tarom Basin: Insights into basin filling and plateau building processes along the northern margin of the Iranian Plateau (Arabia-Eurasia collision zone). Tectonics 40 e2020TC006254.

Popov, S.V., Rögl, F., Rozanov, A.Y., Steininger, F.F., Shcherba, I.G., Kováč, M., 2004. Lithological-paleogeographic maps of Paratethys-10 maps late Eocene to pliocene.

Rahl, J.M., Ehlers, T.A., van der Pluijm, B.A., 2007. Quantifying transient erosion of orogens with detrital thermochronology from syntectonic basin deposits. Earth Planet. Sci. Lett. 256, 147–161.

Rat, J., Mouthereau, F., Brichau, S., Vacherat, A., Fillon, C., Gautheron, C., 2022. Timing and distribution of exhumation in the Ebro basin reveal a plate-scale 10 Ma geodynamic event. Glob. Planet. Chang. 103973 https://doi.org/10.1016/j.gloplacha.2022.103973.

Reiners, P.W., Brandon, M.T., 2006. Using thermochronology to understand orogenic erosion. Annu. Rev. Earth Planet. Sci. 34, 419–466. https://doi.org/10.1146/annurev.earth.34.031405.125202.

Rezaeian, M., Carter, A., Hovius, N., Allen, M.B., 2012. Cenozoic exhumation history of the Alborz Mountains, Iran: new constraints from low-temperature chronometry. Tectonics 31.

Ring, U., Layer, P.W., 2003. High-pressure metamorphism in the Aegean, eastern Mediterranean: underplating and exhumation from the late cretaceous until the Miocene to recent above the retreating Hellenic subduction zone. Tectonics 22.

Rolland, Y., 2017. Caucasus collisional history: review of data from East Anatolia to West Iran. Gondwana Res. 49, 130–146. https://doi.org/10.1016/j.gr.2017.05.005.

Rolland, Y., Perincek, D., Kaymakci, N., Sosson, M., Barrier, É., Avagyan, A., 2012. Evidence for ~80-75Ma subduction jump during Anatolide-Tauride-armenian block accretion and ~48Ma Arabia-Eurasia collision in Lesser Caucasus-East Anatolia. J. Geodyn. 56–57, 76–85. https://doi.org/10.1016/j.jog.2011.08.006.

Romagny, A., Jolivet, L., Menant, A., Bessière, E., Maillard, A., Canva, A., Gorini, C., Augier, R., 2020. Detailed tectonic reconstructions of the Western Mediterranean region for the last 35 Ma, insights on driving mechanisms. Bsgf - Earth Sci Bull. 191, 37. https://doi.org/10.1051/bsgf/2020040.

Royden, L., Faccenna, C., 2018. Subduction orogeny and the late Cenozoic evolution of the Mediterranean Arcs. Annu. Rev. Earth Planet. Sci. 46, 261–289.

Royden, L.H., 1993. Evolution of retreating subduction boundaries formed during continental collision. Tectonics 12, 629–638.

San Jose, M., Rugenstein, J.K.C., Cosentino, D., Faccenna, C., Fellin, M.G., Ghinassi, M., Martini, I., 2020. Stable isotope evidence for rapid uplift of the central Apennines since the late Pliocene. Earth Planet. Sci. Lett. 544, 116376.

Scharf, T.E., Codilean, A.T., De Wit, M., Jansen, J.D., Kubik, P.W., 2013. Strong rocks sustain ancient postorogenic topography in southern Africa. Geology 41, 331–334.

Schildgen, T.F., Cosentino, D., Bookhagen, B., Niedermann, S., Yildirim, C., Echtler, H., Wittmann, H., Strecker, M.R., 2012a. Multi-phased uplift of the southern margin of the Central Anatolian plateau, Turkey: a record of tectonic and upper mantle processes. Earth Planet. Sci. Lett. 317–318, 85–95. https://doi.org/10.1016/j.epsl.2011.12.003.

Schildgen, T.F., Cosentino, D., Caruso, A., Buchwaldt, R., Yldrm, C., Bowring, S.A., Rojay, B., Echtler, H., Strecker, M.R., 2012b. Surface expression of eastern Mediterranean slab dynamics: Neogene topographic and structural evolution of the southwest margin of the Central Anatolian Plateau,Turkey. Tectonics 31. https://doi.org/10.1029/2011TC003021.

Schlunegger, F., Willett, S., 1999. Spatial and temporal variations in exhumation of the central Swiss Alps and implications for exhumation mechanisms. Geol. Soc. LondonSpec. Publ. 154, 157–179.

Schmid, S.M., Bernoulli, D., Fügenschuh, B., Matenco, L., Schefer, S., Schuster, R., Tischler, M., Ustaszewski, K., 2008. The Alps-Carpathians-Dinarides-connection: a correlation of tectonic units. Swiss J. Geosci. 101, 139–183.

Şengör, A.M.C., 1984. The cimmeride orogenic system and the tectonics of Eurasia. Geol. Soc. London Spec. Publ. 195.

Şengör, A.M.C., Tüysüz, O., Imren, C., Sakınç, M., Eyidoğan, H., Görür, N., Le Pichon, X., Rangin, C., 2005. The North Anatolian fault: a new look. Annu. Rev. Earth Planet. Sci. 33, 37–112.

Serpelloni, E., Vannucci, G., Pondrelli, S., Argnani, A., Casula, G., Anzidei, M., et al., 2007. Kinematics of the Western Africa-Eurasia plate boundary from focal mechanisms and GPS data. Geophys. J. Int. 169 (3), 1180–1200. https://doi.org/10.1111/j.1365- 246X.2007.03367.x.

Seton, M., Müller, R.D., Zahirovic, S., Gaina, C., Torsvik, T.H., Shephard, G., Talsma, A., Gurnis, M., Turner, M., Maus, S., Chandler, M., 2012. Global continental and ocean basin reconstructions since 200Ma. Earth-Sci.Rev. 113, 212–270. https://doi.org/10.1016/j.earscirev.2012.03.002.

Seton, Maria, Müller, R.D., Zahirovic, S., Gaina, C., Torsvik, T.H., Shephard, G., Talsma, A., Gurnis, M., Turner, M., Maus, S., Chandler, M., 2012. Global continental and ocean basin reconstructions since 200Ma. Earth Sci.Rev. 113, 212–270. https://doi.org/10.1016/j.earscirev.2012.03.002.

Seward, D., Mancktelow, N.S., 1994. Neogene kinematics of the central and western Alps: evidence from fission-track dating. Geology 22, 803–806.

Skolbeltsyn, G., Mellors, R., Gök, R., Türkelli, N., Yetirmishli, G., Sandvol, E., 2014. Upper mantle S wave velocity structure of the East Anatolian-Caucasus region. Tectonics 33, 207–221. https://doi.org/10.1002/2013TC003334.

Soumaya, A., Ben Ayed, N., Rajabi, M., Meghraoui, M., Delvaux, D., Kadri, A., Braham, A., 2018. Active faulting geometry and stress pattern near complex strike-slip systems along the Maghreb Region: Constraints on active convergence in the Western Mediterranean. Tectonics 37 (9), 3148–3173.

Srodoń, J., Anczkiewicz, A.A., Dunkl, I., Vlahović, I., Velić, I., Tomljenović, B., Kawiak, T., Banaś, M., von Eynatten, H., 2018. Thermal history of the central part of the Karst Dinarides, Croatia: combined application of clay mineralogy and low-T thermochronology. Tectonophysics 744, 155–176. https://doi.org/10.1016/j.tecto.2018.06.016.

Stampfli, G.M., Borel, G.D., 2002. A plate tectonic model for the Paleozoic and Mesozoic constrained by dynamic plate boundaries and restored synthetic oceanic isochrons. Earth Planet. Sci. Lett. 196, 17–33. https://doi.org/10.1016/S0012-821X(01)00588-X.

Tadayon, M., Rossetti, F., Zattin, M., Calzolari, G., Nozaem, R., Salvini, F., Faccenna, C., Khodabakhshi, P., 2019. The long-term evolution of the Doruneh Fault region (Central Iran): a key to understanding the spatio-temporal tectonic evolution in the hinterland of the Zagros convergence zone. Geol. J. 54, 1454–1479.

Tadayon, M., Rossetti, F., Zattin, M., Nozaem, R., Calzolari, G., Madanipour, S., Salvini, F., 2017. The post-eocene evolution of the Doruneh Fault region (central Iran): the intraplate response to the Reorganization of the Arabia-Eurasia collision zone. Tectonics 36, 3038–3064.

Tarantola, A., 2005. Inverse problem theory and methods for model parameter estimation, Society for Industrial Mathematics.

Teixell, A., Labaume, P., Ayarza, P., Espurt, N., de Saint Blanquat, M., Lagabrielle, Y., 2018. Crustal structure and evolution of the Pyrenean-Cantabrian belt: a review and new interpretations from recent concepts and data. Tectonophysics 724, 146–170.

Thomson, S.N., Brandon, M.T., Reiners, P.W., Zattin, M., Isaacson, P.J., Balestrieri, M.L., 2010. Thermochronologic evidence for orogen-parallel variability in wedge kinematics during extending convergent orogenesis of the northern Apennines, Italy. Bulletin 122, 1160–1179.

Topuz, G., Candan, O., Zack, T., Yilmaz, A., 2017. East Anatolian plateau constructed over a continental basement: no evidence for the East Anatolian accretionary complex. Geology 45, 791–794. https://doi.org/10.1130/G39111.1.

Ustaszewski, K., Kounov, A., Schmid, S.M., Schaltegger, U., Krenn, E., Frank, W., Fügenschuh, B., 2010. Evolution of the Adria-Europe plate boundary in the northern Dinarides: from continent-continent collision to back-arc extension. Tectonics 29.

Vacherat, A., Mouthereau, F., Pik, R., Bellahsen, N., Gautheron, C., Bernet, M., Daudet, M., Balansa, J., Tibari, B., Pinna Jamme, R., 2016. Rift-to-collision transition recorded by tectonothermal evolution of the northern Pyrenees. Tectonics 35, 907–933.

van Hinsbergen, D.J.J., Torsvik, T.H., Schmid, S.M., Maţenco, L.C., Maffione, M., Vissers, R.L.M., Gürer, D., Spakman, W., 2020. Orogenic architecture of the Mediterranean region and kinematic reconstruction of its tectonic evolution since the Triassic. Gondwana Res. 81, 79–229. https://doi.org/10.1016/j.gr.2019.07.009.

Vergés, J., Fernàndez, M., 2012. Tethys-Atlantic interaction along the Iberia-Africa plate boundary: the Betic-Rif orogenic system. Tectonophysics 579, 144–172. https://doi.org/10.1016/j.tecto.2012.08.032.

Vernon, A.J., Van Der Beek, P.A., Sinclair, H.D., Rahn, M.K., 2008. Increase in late Neogene denudation of the European Alps confirmed by analysis of a fission-track thermochronology database. Earth Planet. Sci. Lett. 270, 316–329.

Wagner, G.A., 1979. Correction and interpretation of fission track ages. In: Lectures in Isotope Geology. Springer, pp. 170–177.
Westerhold, T., Marwan, N., Drury, A.J., Liebrand, D., Agnini, C., Anagnostou, E., Barnet, J.S.K., Bohaty, S.M., De Vleeschouwer, D., Florindo, F., 2020. An astronomically dated record of Earth's climate and its predictability over the last 66 million years. Science (80-.) 369, 1383–1387.
Whipple, K.X., 2009. The influence of climate on the tectonic evolution of mountain belts. Nat. Geosci. 2, 97.
Willett, S.D., Slingerland, R., Hovius, N., 2001. Uplift, shortening, and steady state topography in active mountain belts. Am. J. Sci. 301 (4–5), 455–485.
Willett, S.D., 2010. Late Neogene erosion of the Alps: a climate driver? Annu. Rev. Earth Planet. Sci. 38, 411–437.
Willett, S.D., Brandon, M.T., 2013. Some analytical methods for converting thermochronometric age to erosion rate. Geochem.Geophys. Geosyst. 14, 209–222. https://doi.org/10.1029/2012GC004279.
Willett, S.D., Herman, F., Fox, M., Stalder, N., Ehlers, T.A., Jiao, R., Yang, R., 2021. Bias and error in modelling thermochronometric data: resolving a potential increase in Plio-Pleistocene erosion rate. Earth Surf. Dyn. 9, 1153–1221.
Willett, S.D., Schlunegger, F., Picotti, V., 2006. Messinian climate change and erosional destruction of the central European Alps. Geology 34, 613–616. https://doi.org/10.1130/G22280.1.
Zachos, J.C., Dickens, G.R., Zeebe, R.E., 2008. An early Cenozoic perspective on greenhouse warming and carbon-cycle dynamics. Nature 451, 279–283. https://doi.org/10.1038/nature06588.
Zachos, J., Pagani, M., Sloan, L., Thomas, E., Billups, K., 2001. Trends, rhythms, and aberrations in global climate 65 Ma to present. Science 292 (5517), 686–693.
Zanchetta, S., Malusà, M.G., Zanchi, A., 2015. Precollisional development and Cenozoic evolution of the Southalpine retrobelt (European Alps). Lithosphere 7, 662–681.
Zanchi, A., Zanchetta, S., Garzanti, E., Balini, M., Berra, F., Mattei, M., Muttoni, G., 2009. The Cimmerian evolution of the Nakhlak-Anarak area Central Iran and its bearing for the reconstruction of the historyof the Eurasian margin. Geol. Soc. Spec. Publ. 312, 261–286. https://doi.org/10.1144/SP312.13.
Zhang, H., Henderson-Sellers, A., McGuffie, K., 2001. The compounding effects of tropical deforestation and greenhouse warming on climate. Clim. Chang. 49, 309–338.